REVIEW OF PALEOLIQUEFACTION DATA, EVALUATION OF SCENARIO EARTHQUAKES, AND ESTIMATION OF SOURCE AREAS, MAGNITUDES, AND RECURRENCE OF LARGE EARTHQUAKES IMPACTING PUERTO RICO AND THE U.S. VIRGIN ISLANDS

Final Technical Report

Research supported by the U.S. Geological Survey,
Department of the Interior,
EHP Award No. G21AP10006

Principal Investigator
Martitia P. Tuttle

Research Associates
Kathleen Dyer-Williams
Kathleen B. Tucker

M. Tuttle & Associates
P.O. Box 345
Georgetown, ME 04548
Telephone: (207) 371-2007
E-mail: mptuttle@earthlink.net
URL: http://www.mptuttle.com

Project Period: 1/1/2021 to 6/30/2022

Program Element I: National and Regional Earthquake Hazards Assessments

Key Words: Paleoliquefaction, Paleoearthquakes, Age Dating

REVIEW OF PALEOLIQUEFACTION DATA, EVALUATION OF SCENARIO EARTHQUAKES, AND ESTIMATION OF SOURCE AREAS, MAGNITUDES, AND RECURRENCE OF LARGE EARTHQUAKES IMPACTING PUERTO RICO AND THE U.S. VIRGIN ISLANDS

Principal Investigator
Martitia P. Tuttle

Research Associates
Kathleen Dyer-Williams
Kathleen B. Tucker

M. Tuttle & Associates
P.O. Box 345
Georgetown, ME 04548
Telephone: (207) 371-2007
E-mail: mptuttle@earthlink.net
URL: http://www.mptuttle.com

Abstract

More than ninety liquefaction features found along rivers in the northwestern and north-central Puerto Rico provide a record of large earthquakes during the past 5,400 years. The liquefaction features, including sand dikes, sand blows, and sand sills, are attributed to the historical earthquakes of 1918, 1787, and 1670 and two paleoearthquakes circa A.D. 1304-1508 and 1201-410 B.C. Various scenario earthquakes are evaluated using liquefaction potential analysis, and events are identified that best match observed liquefaction along the rivers. Using locations from the Advanced National Seismic System (ANSS) and U.S. Geological Survey (USGS) earthquake catalogs, the evaluations suggest a **M** 7.4 for the 1918 earthquake, a **M** 7.7 for the 1787 earthquake, and a **M** 6.2 located on the Cerro Godin fault zone north of Añasco for the 1670 earthquake. For the A.D. 1304-1508 and 1201-410 B.C. paleoearthquakes, the analyses suggest a **M** 8.5 produced by the eastern Septentrional fault zone and a **M** 7.8 produced by the Bowin fault zone, respectively. If the paleoearthquakes did occur on these structures, the findings indicate a recurrence time of at least 514-718 years and possibly much longer for great earthquakes on the eastern Septentrional fault zone, and at least 2,432-3,223 years for very large earthquakes on the Bowin fault zone.

Introduction

Puerto Rico and the Virgin Islands (PRVI) region, located within a diffuse and complex boundary zone between the North American and Caribbean tectonic plates, has long been recognized as having significant seismic hazards (Figure 1; Asencio, 1980; McCann, 1985; Moya and McCann, 1991; Mueller et al., 2003 and 2010). Several large to very large earthquakes have struck the PRVI region in the past 400 years. These include a moment magnitude, **M** ~7.9 plate interface (Hispaniola segment) event in 1946 northeast of Hispaniola; a **M** ~7.7 plate interface (Puerto Rico segment) event in 1943 northwest of Puerto Rico; a **M** ~7.5 Mona Passage event in 1918 northwest of Puerto Rico; a **M** ~7.3 Anegada Passage event in 1867 east of Puerto Rico; a **M** ~8.0-8.2 plate interface (Puerto Rico segment) event in 1787 north of Puerto Rico; and a **M** ~6 event in 1670 probably in western Puerto Rico (Figure 1; e.g., Reid and Taber, 1919; McCann, 1985 and 2003; Dolan and Wald, 1998; Mueller et al., 2003 and 2010; Doser et al., 2005; LaForge and McCann, 2005; Prentice and Mann, 2005; ten Brink et al., 2011; Flores et al., 2012). A reassessment of the 1787 event estimated an intensity magnitude of 6.4-6.9 and proposed three possible locations, including southwest of Puerto Rico near the Muertos Trough, the north coast of the Puerto Rico, and Main Ridge near the Puerto Rico Trench (ten Brink et al., 2011).

As demonstrated by the historical record of earthquakes, coastal areas of PRVI have been subjected to strong ground shaking, liquefaction, and tsunami inundation caused by large earthquakes. The 1946 plate interface event triggered a tsunami that washed ashore in northwestern Puerto Rico and northeastern Dominican Republic where it killed ~1800 people, and was recorded at San Juan (Figure 1; Lander et al., 2002; Grindlay et al., 2005a). It also induced liquefaction in the Cibao river valley in eastern Dominican Republic (Lynch and Bodle, 1948; Tuttle et al., 2003). In contrast, the 1943 plate interface earthquake was strongly felt throughout Puerto Rico but caused no structural damage (McCann, 2003). The shaking may have been of Modified Mercalli intensity V which would not have been strong enough to induce liquefaction. In addition, no tsunami was observed for this event (O'Loughlin and Lander, 2003). The 1918 earthquake and related tsunami had their greatest impact on the western coast of Puerto Rico, killing at least 114 persons and causing $4 million in damage (Reid and Taber, 1919). This earthquake also induced liquefaction near Aguadilla and in the Río Grande de Añasco valley (Figure 1; Moya and McCann, 1991). The 1867 earthquake produced a tsunami that was especially damaging to the U.S. Virgin Islands, including St. Thomas, and also washed ashore in southeastern Puerto Rico (Lander et al., 2002). The 1670 earthquake caused damage in San Germán and San Juan (McCann, 2003) and is thought to be responsible for liquefaction features uncovered at an archeological site east of Mayagüez on the floodplain of the Yaquez River (Moya, 1998). Paleotsunami deposits dating to A.D. 1270-1410 and 820-400 B.C. were found in a coastal lagoon in Aguadilla in northwestern Puerto Rico, suggesting earlier large offshore earthquakes (Moya, 1999).

Between 2000 and 2011, several paleoliquefaction studies were conducted in western, northern, and eastern Puerto Rico to provide information about past earthquakes and help reduce uncertainties in seismic hazard assessments (Tuttle et al., 2005a and 2005b; Tuttle and Dyer-Williams, 2006 and 2008; Tuttle, 2011). In this paper, the results of those studies are brought together and the ages of liquefaction features are reinterpreted. In addition, scenario earthquakes

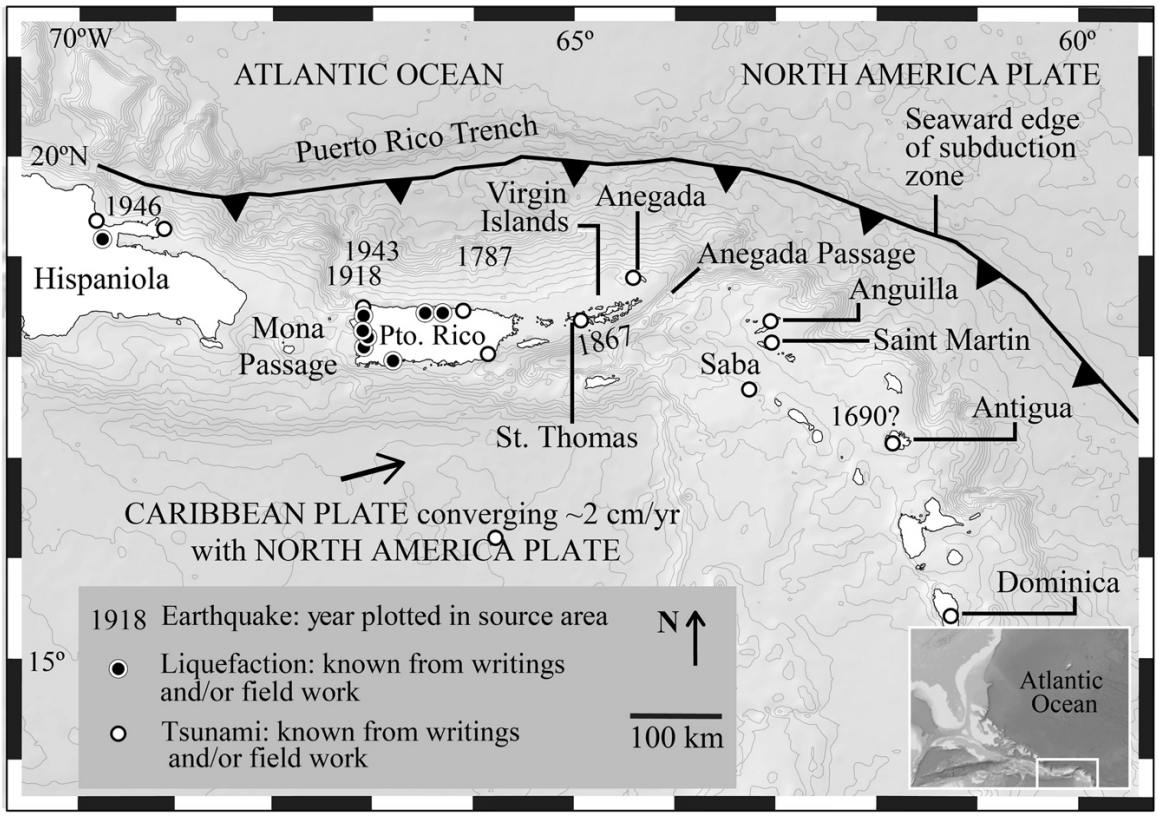

Figure 1. Tectonic map of northeastern Caribbean, showing locations of large historical earthquakes relative to Puerto Rico and the Virgin Islands and of earthquake-related liquefaction and tsunamis. Inset shows location of map area (white rectangle) southeast of southeastern U.S. (modified from Fuentes et al., 2017).

are reevaluated using liquefaction potential analysis and updated ground motion prediction equations and those results, along with the size and distribution of similar-age liquefaction features, are interpreted in terms magnitudes, source areas, and recurrence times of past earthquakes.

Recent events have heightened the awareness and concern about earthquake potential and related hazards posed by sources in the PRVI region. Following the devastating 2004 Aceh-Andaman, Indonesia, mega-thrust (**M** > 9) earthquake and resulting tsunami, the Puerto Rico Trench (PRT) and the Lesser Antilles subduction zone were identified as possible sources of great earthquakes and related tsunamis that could endanger the PRVI region as well as the U.S. and Canadian Atlantic coasts (ten Brink et al., 2004 and 2014; Atlantic and Gulf of Mexico Tsunami Hazard Assessment Group, 2008; Grilli et al., 2022). On January 7, 2020, a **M** 6.4, earthquake struck about 8 km off the southwestern coast of Puerto Rico, killed at least four people, induced liquefaction in alluvium and beach deposits along 35 km of the southwestern coast, and caused widespread damage estimated at $800 million (Allstadt et al., 2022; Miranda et al., 2020). Given that most of the population (~3 million U.S. citizens) and urban development is concentrated in coastal areas, the PRVI region is at risk from future earthquakes.

Offshore and Onshore Earthquake Sources

Offshore sources are thought to pose the most significant earthquake hazard in the PRVI region. Possible seismic sources related to the main plate boundary include normal faults on the outer wall of the Puerto Rico trench, thrust faults of the plate interface south of the Puerto Rico Trench, intraslab faults within the subducting North America plate, and strike-slip faults subparallel to the Puerto Rico Trench north and northwest of Puerto Rico (Figure 2). The latter include the eastern Septentrional fault zone, a plate-boundary structure extending from Hispaniola southeastward to Mona Canyon, the Bunce fault zone (formerly the North Puerto Rico Slope fault zone), and the Bowin fault zone (formerly South Puerto Rico Slope fault zone and a possible eastward extension of the eastern Septentrional fault zone). Other earthquake sources include zones of east-west extension within the Mona Passage west of Puerto Rico and the Anegada Passage east of the island, as well as the Muertos Trough, the southern boundary of the PRVI microplate, south of Puerto Rico.

Major onshore fault zones include the Great Northern Puerto Rico fault zone (GNPRFZ) and the Great Southern Puerto Rico fault zone (GSPRFZ) (Figure 2). The GNPRFZ is a major northwest to west-northwest trending, left-lateral strike-slip fault system that crosses the northern part of the island about 20 km south of San Juan, with one or more splays approaching the suburbs of the city. The fault zone offsets lower Cretaceous to Eocene rocks and is overlain by middle Tertiary strata along the north coast (e.g., Monroe, 1980). Even though small shallow earthquakes are spatially associated with it (McCann, 1985), the fault zone is thought to be inactive (Geomatrix, 1988). A paleoseismic study of the fault zone in eastern Puerto Rico found no evidence of fault movement at least during the Holocene (Williams and Tuttle, 2010).

The GSPRFZ is another major northwest-trending, left-lateral strike-slip fault system that crosses southern and western Puerto Rico (Figure 2). It is also characterized by dip-slip displacement in the south-central part of the island (Geomatrix, 1988). Field investigations of the GSPRFZ by the Department of Geology at the University of Puerto Rico documented two phases of normal faulting, one phase during the Oligocene and the other after the Oligocene. In the 1970s, trenching of faults in the system uncovered evidence of Quaternary faulting in the south (Geomatrix, 1988). Single- and multi-channel seismic data collected across the offshore extension of the Cerro Godin fault zone, a member of the GSPRFZ located ~10 km north of Mayaguez, suggest fault displacements of Pliocene and possibly Holocene sediment (Prentice et al., 2003a). Although geomorphic features suggest possible late Quaternary right-lateral displacement, no unequivocal evidence of faulting has been found in excavations across projected surface traces of the inferred faults (Mann et al., 2005).

In southwestern Puerto Rico, an area of shallow seismicity (Asencio, 1980; McCann, 1985), the South Lajas fault was found to have ruptured the surface twice in the past 7,500 years (Figure 2; Prentice et al., 2000; Prentice and Mann, 2005). Based on an estimated total fault length of 50 km, these earthquakes may have been of **M** 7.0 (LaForge and McCann, 2005). This finding strongly influenced the seismic hazard map for the southwestern part of the island (Figure 3). Subsequently, the North Boqueron Bay-Punta Montalva fault zone was mapped across the Lajas Valley and was interpreted as a seismically active, major through-going, left-lateral strike-slip fault zone (Roig-Silva et al., 2013).

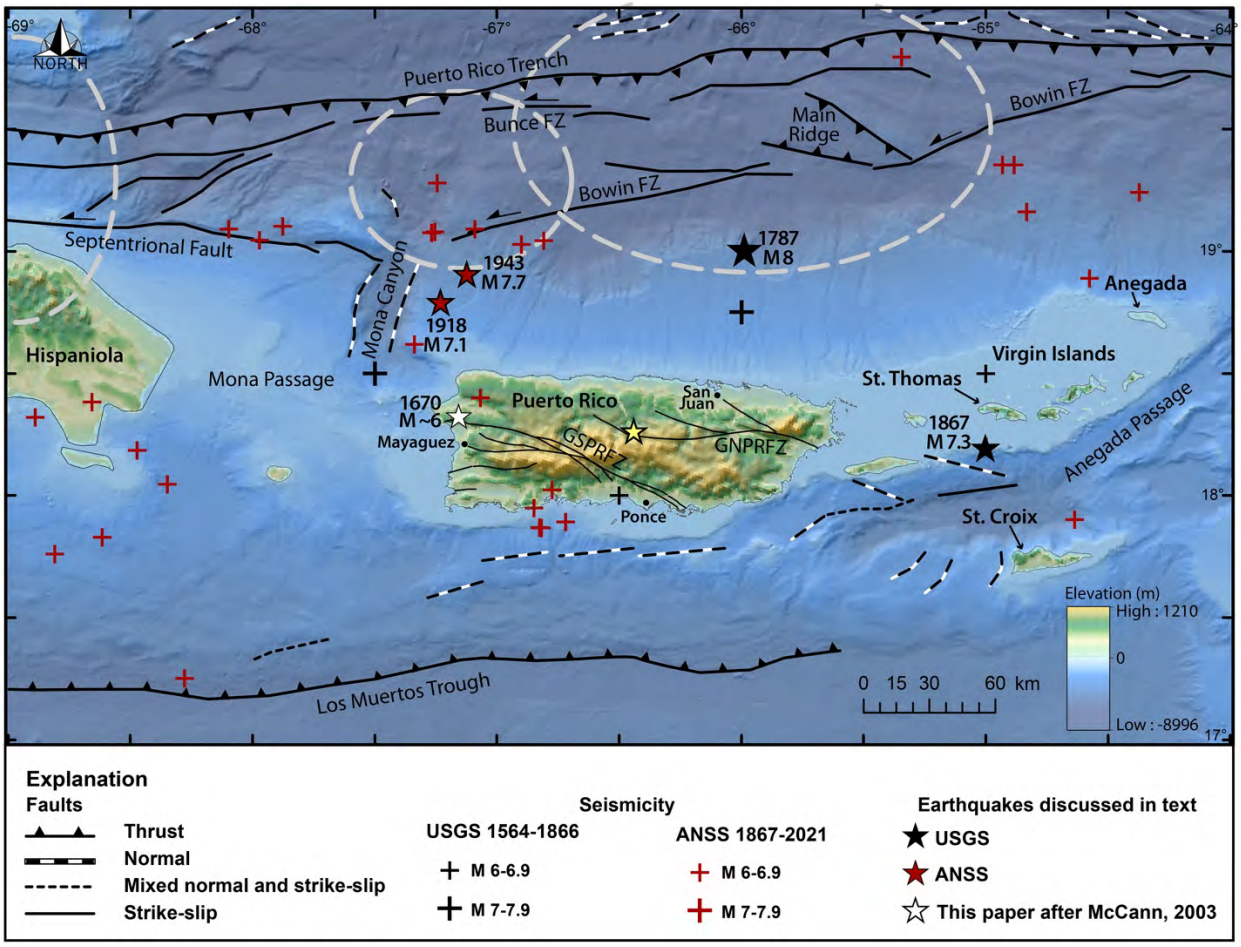

Figure 2. Regional map of Puerto Rico and the Virgin Islands, showing seismicity from A.D. 1564-1866 (from Mueller et al., 2003) and A.D. 1867-2021 (from U.S. Geological Survey-ANSS, 2017) as well as onshore faults (Briggs, 1964; Monroe, 1980; Geomatrix, 1988; Mann et al., 2005; Prentice and Mann, 2005) and offshore faults (Grindlay et al., 2005b; ten Brink et al., 2011). Dashed white lines represent approximate rupture areas of historic earthquakes (left to right - 1946, 1943, and 1787; after McCann, 1985; Dolan and Wald, 1998; Doser et al., 2005).

Seismic Hazard Assessment

For the probabilistic seismic hazard assessment of Puerto Rico and the U.S. Virgin Islands, the subduction interface was subdivided into the Puerto Rico and Hispaniola segments (Mueller et al., 2003 and 2010). Based on a GPS-determined slip rate of ~17 mm/yr and about 20% seismic coupling, interface earthquakes on the Puerto Rico segment was modeled as **M** 7.9 ruptures with 190 yr recurrence times (Jansma et al., 2000). For San Juan, the Puerto Rico segment of the subduction interface, deep seismicity, and shallow seismicity, equally contribute to the seismic hazard in the ground-motion range between 2,500- and 500-year return times (Figure 3; Mueller et al., 2003 and 2010).

A major concern in seismic hazard assessment of Puerto Rico is the importance of the eastern Septentrional fault zone and its possible eastward extension, the Bowin fault zone, both of which

are closer to Puerto Rico than the plate interface (Mueller et al., 2003 and 2010). The eastern Septentrional fault zone apparently does not offset Mona Canyon and has not produced any major earthquakes during the historical period. The 350-km length of the eastern Septentrional fault zone correlates with an earthquake of **M** 8.0, and the 160-km length of the Bowin fault zone correlates with a **M** 7.6 earthquake (Wells and Coppersmith, 1994). Estimates of the slip rate for the eastern Septentrional fault zone and the Bowin fault zone range from 9 mm/yr to 2 mm/yr and 9 mm/yr to 0 mm/yr, respectively (e.g., Prentice et al., 2003b; LaForge and McCann, 2005). In the 2003 seismic hazard assessment for Puerto Rico, the eastern Septentrional fault zone was assigned a slip rate of 2 mm/yr which implies a recurrence time of 3,600 years for **M** 8 earthquakes; and the Bowin fault zone was assigned a slip rate of 1 mm/yr which implies a recurrence time of 3,900 years for **M** 7.6 earthquakes.

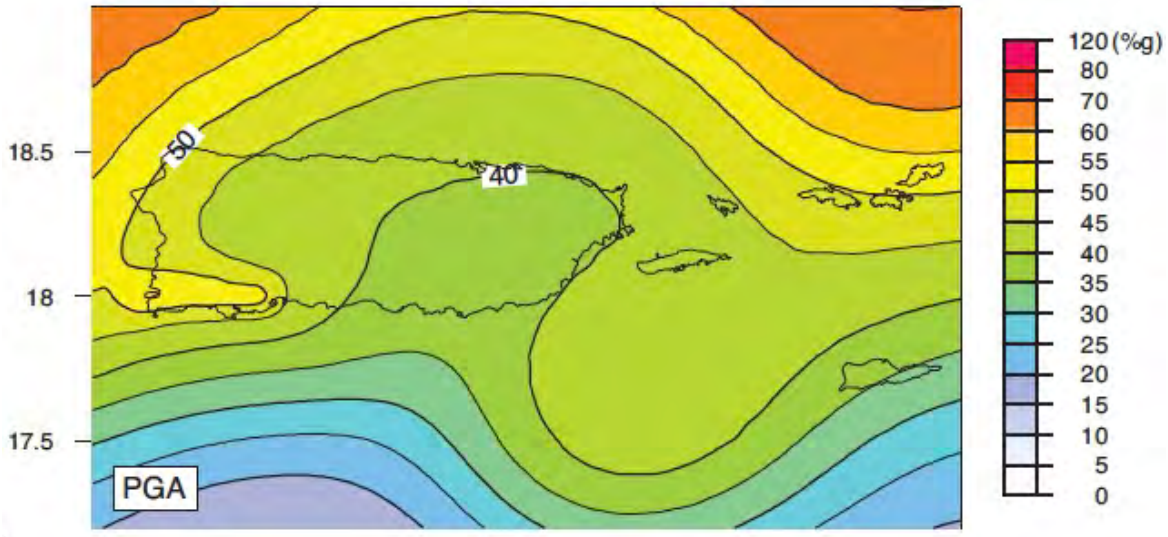

Figure 3. Map of PRVI area showing probabilistic peak ground acceleration (% g), including contributions from all modeled sources, for an exceedance probability of 2% in 50 years (about 2,500-year return period) (from Mueller et al., 2010). Note influence of Lajas fault in southwestern Puerto Rico on hazard map, illustrating potential benefit of paleoseismic studies.

Because most of the major seismogenic structures are located offshore of Puerto Rico, locations and magnitudes of the historic earthquakes are poorly constrained (Doser et al., 2005) and recurrence rates are essentially unknown (Mueller et al., 2003 and 2010). Studies of earthquake-induced liquefaction features can help to reduce uncertainties in seismic hazard assessments by providing information about large earthquakes in the past (Tuttle et al., 2019). By dating liquefaction features, timing of the causative earthquakes can be estimated. The sizes and areal distribution of similar-age features, combined with evaluation of scenario earthquakes, can be used to estimate source areas and magnitudes of the earthquakes.

Tsunami geology studies in the northeastern Caribbean have identified likely tsunami deposits on several islands, including Anegada (Atwater et al., 2011 and 2017; Pilarczyk and Reinhardt, 2012), St. Thomas (Fuentes et al., 2017; Tuttle and Fuentes, 2021), Anguilla (Biguenet et al., 2021), and Puerto Rico (Moya, 1999). Many of the deposits are attributed to one or several very large earthquakes (**M** 8-9) resulting from rupture of the North America-Caribbean plate interface or

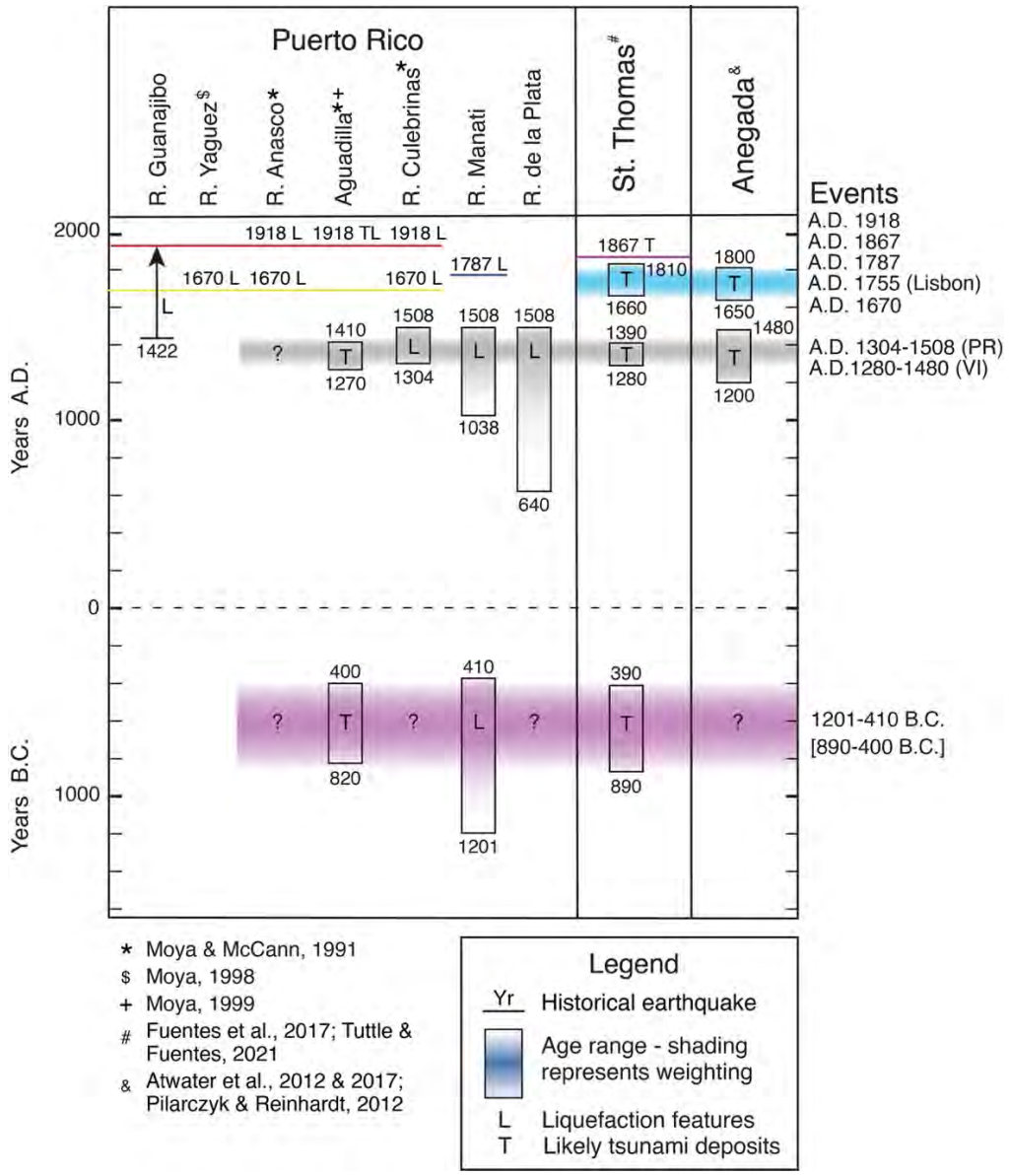

Figure 4. Spacetime diagram of liquefaction features and tsunami deposits in the PRVI region.

outer-rise normal faults between A.D. 1200-1500 (Figure 4; Cordrie et al., 2022; Wei et al., 2016; Wei, 2022). In addition, tsunami deposits dating between 890-400 B.C. have been found in Aguadilla in northwestern Puerto Rico (Moya, 1999) and on St. Thomas (Fuentes et al., 2017; Tuttle and Fuentes, 2021), but not on Anegada which has a shorter tsunami record (Figure 4). The combined liquefaction and tsunami records can provide a longer and broader view of the regional impacts of offshore events and contribute to understanding of source areas, magnitudes, and recurrence of large earthquakes.

Compilation and Reinterpretation of Liquefaction Data

Between 2000 and 2011, several paleoliquefaction studies were conducted in western, northern, and eastern Puerto Rico that involved surveying major rivers for earthquake-induced liquefaction

features. Prior to the surveys, river segments were selected based on the accounts of liquefaction during historical earthquakes, the mapped occurrence of Quaternary alluvium (Figure 5; Bawiec, 1999), and reconnaissance confirming cutbank exposure of sediment prone to earthquake-induced liquefaction and the formation of liquefaction features. More specifically, sedimentary conditions ideal for paleoliquefaction studies include sandy sediment capped by or interbedded with relatively impermeable sediment that promotes the increase of porewater pressure in and liquefaction of saturated sandy sediment during ground shaking (Fiegel and Kutter, 1994; Tuttle et al., 2019). Segments of the following rivers were selected for survey: Grande de Añasco, Culebrinas, Guanijibo, Grande de Arecibo, Grande de Manati, Cibuco, de la Plata, Canovanas, Espiritu Santo, Mameyes, Fajardo, Blanco, Humacao, Maunabo, Grande de Loíza, Gurabo, and Valenciano (Figure 5). No river segments were selected along the southern coast because cutbank exposures were rare in predominantly sandy sediment.

During the surveys, totaling more than 160 km, sedimentary conditions were found to be suitable for the formation of liquefaction features along most of the selected river segments, except for Río Mameyes, Río Fajardo, and Río Grande de Loiza, and less than ideal along Río Grande de Arecibo and Río Cibuco. More than ninety liquefaction features were discovered along rivers in western and north-central Puerto Rico (Figure 6). No liquefaction features were found along any of the rivers in northeast and eastern Puerto Rico. Information collected during the surveys includes cutbank exposure and sedimentary conditions along the rivers, presence of liquefaction features, and if so, their locations, positions in the cutbanks, and characteristics, such as type (i.e., sand dike, sand blow, soft-sediment deformation), measured size, and weathering. This information is summarized in Table 1 and presented in detail in Table S1 of the Supplement. All liquefaction features are similar to features resulting from liquefaction induced by modern earthquakes and meet the identification criteria presented in a recent review paper (Tuttle et al., 2019).

Maps for the entire island (Figures 5 and 6) and more detailed maps for the five rivers along which liquefaction features were found (Figures S1-S5) show river segments that were surveyed for liquefaction features and the locations, sizes, and estimated ages of liquefaction features found during the surveys. While making the GIS-based maps for the Río Grande de Añasco, Río Culebrinas, and Río Guanajibo valleys, it was discovered that the GPS coordinates for liquefaction features recorded in the year 2000 were inaccurate often by 10s of meters, plotting far from the river's course at the time. To correct the coordinates, locations of liquefaction features were identified on Google Earth satellite imagery by using 7 ½ minute quadrangle maps on which the locations of liquefaction features were marked in 2000 and field notes. The corrected locations of liquefaction features are provided in Table S1 and shown on Figures 6 and Figures S1-S5.

Previously, organic samples collected in the field were dated for the purpose of estimating the age of sediment and of liquefaction features exposed in river cutbanks. Radiocarbon dating using the accelerator mass-spectrometry (AMS) technique was performed by Beta Analytic, Inc., resulting in conventional ages with uncertainties of +/- 40 years. The ages were calibrated using either CALIB or the Pretoria procedure. Over the past twenty years, both the calibration method and the database used in the calibration have evolved. Therefore, for this paper, all conventional ages were recalibrated using the probability method of Bronk Ramsey (2009) and the updated

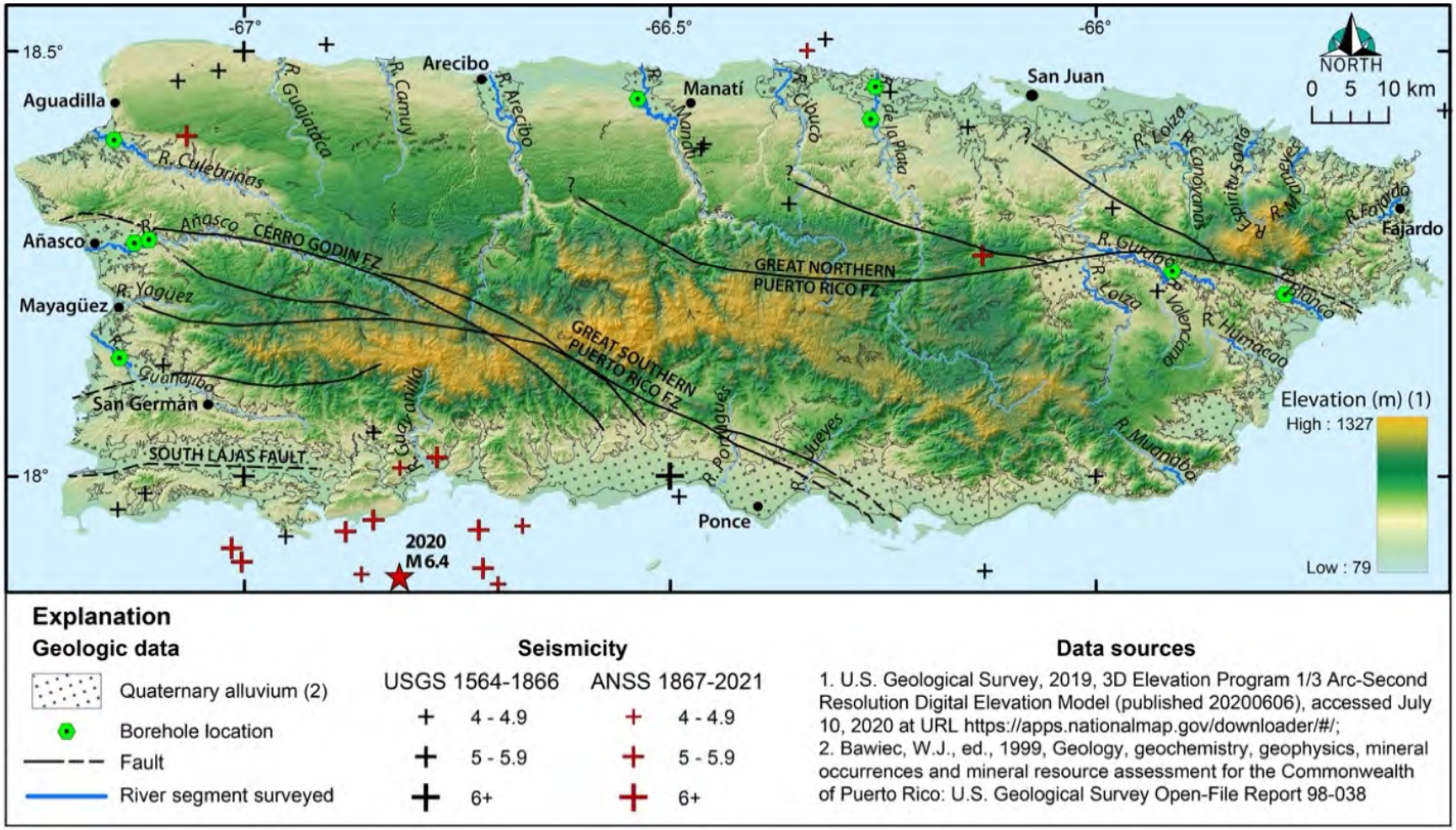

Figure 5. Map of Puerto Rico showing distribution of Quaternary alluvium, borehole locations, and portions of major rivers surveyed for earthquake-induced liquefaction features. Onshore faults indicated by heavy black lines (dashed where inferred) (from Briggs, 1964; Monroe, 1980; Geomatrix, 1988; Mann et al., 2005; and Prentice and Mann, 2005).

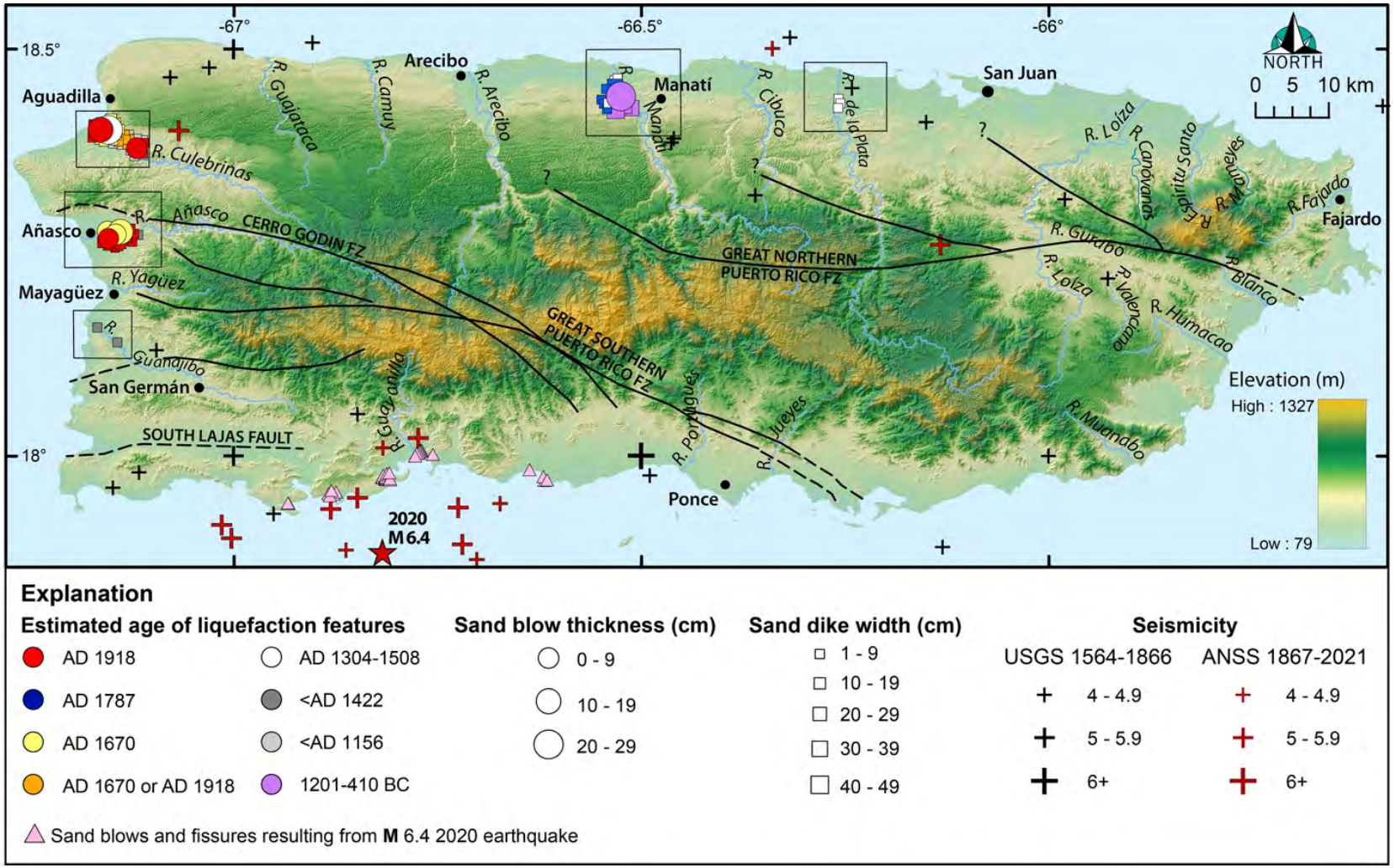

*Figure 6. Island map showing locations, sizes, and estimated ages of earthquake-induced liquefaction features. Black rectangles indicate areas of maps shown in Figures S1-S5. Liquefaction resulting from **M** 6.4, January 7, 2022 earthquake (from Allstadt et al., 2022).*

Table 1. River surveys, sediment conditions, and earthquake-induced liquefaction features.

River Surveys	Cutbank Exposure	Suitable Conditions	Sediment Age*	Liquefaction Features	Age Estimate of Features
West Coast					
Grande de Añasco 13 km	Good to excellent in frequent bends, especially along lowermost 6 km surveyed, 3-5 high	Yes; Holocene alluvium; recent silt overlying reddish brown silt & clayey silt with lenses of sand & interbedded silt, clayey silt, sand, & pebbley sand; buried soils	A.D. 1422 from RGA4-C3; charred material collected 2.03 m BTC	Four sand blows, 0.5-12 cm thick; thirty sand dikes, 0.4-20 cm wide	A.D. 1918; A.D. 1670
Culebrinas 14 km	Good to excellent in frequent bends along upper & lower thirds of river, 3-8 m high; middle portion mostly vegetated; poor exposure along lower 1 km	Yes; Holocene alluvium; reddish brown silt, few interbeds of sand, overlying sand & pebbly sand; 2-7 buried soils	A.D. 1053 from RC101-C1; charred material collected 7.2 m BTC	Three sand blows, 1-20 cm thick; forty-one sand dikes, 0.5-23 cm wide	A.D. 1918; A.D. 1304-1508
Guanijibo 10	Good in bends, 2.5-3.3 m high; poor exposure along lowermost 2 km	Yes; Holocene alluvium; silt & clayey silt with interbeds of sand; 3 buried soils; likely similar in age to sediment along Río Grande de Añasco	No dates	Two sand dikes, 0.5-3 cm wide	<A.D. 1400
Northwest Coast					
Grande de Arecibo 16.7 km	Good to excellent in river bends, 2-6 m high; few exposures along straight sections; otherwise vegeta-ted	Yes, but not ideal due to abundance of pebbles, cobbles, & boulders; Holocene alluvium; light brown silt with lenses of sand overlying sand, pebbles & cobbles; 1-2 buried soils	No dates	No	Not applicable
Grande de Manati 22 km	Excellent in frequent river bends along upper two-thirds of river, 4-7 m high; poorer exposure along lower 2 km, 1-4 m high	Yes; Holocene alluvium; upstream third: reddish silt & interbedded sand overlying pebbles & cobbles; multiple buried soils; downstream two-thirds: reddish silt & clayey silt overlying silty sand & sand; 2-6 buried soils	3330 B.C. from RM2N-C1; charred material collected 5.15 m BTC	One sand blow, 22 cm thick; eleven sand dikes, 0.4-40 cm wide, two sand sills, 3 cm thick; graben associated	A.D.1787; A.D.1304-1508; 1201-410 B.C.

				with large dike	
Cibuco 8 km	Fair in most bends along upstream half, 3-4 m high; exposure less frequent along channelized downstream half; lower 1.5 km mostly vegetated	Probably, but not ideal due to sparse sand interbedded with silt; Holocene alluvium & back-swamp deposits; reddish brown silt, occasional interbed of sand with granules and pebbles; 3 buried soils	No dates	No	Not applicable
de la Plata 7 km	Good to excellent in bends along upstream third, 4-5 m high; excellent along middle third, 2-5 m high; good exposure in few bends along downstream third, 2 m high	Yes; Holocene alluvium; reddish brown silt, interbedded silt & sand; up to 5 buried soils	A.D. 640 from RLP10-C2; charred material collected 2.2 m BTC	Three sand dikes, 0.5-1.5 cm wide; graben associated with largest dike	A.D. 1304-1508
Northeast Coast					
Canovanas, tributary to Grande de Loíza 3.7 km	Good to excellent in most river bends, 4-5 m high	Yes, Holocene alluvium; upstream portion: reddish silt overlying interbedded silt & silty sand followed by pebbley sand & pebbles; downstream portion: reddish brown silt overlying reddish silt with at least 1 buried soil	No dates	No	Not applicable
Espiritu Santo 3.2 km	Good in bends along upstream third, 5-6 m high; otherwise poor due to vegeta-tion; mangroves along lower 0.5 km	Yes; Holocene alluvium; upstream third: interbed-ded silt & sandy silt containing buried soils followed by pebbley sand; downstream two-thirds: interbedded silt & sand	A.D. 382 from RGR1-W1; charred material collected 6.3 m BTC	No	Not applicable
Mameyes 4.5 km	Good in bends along upper half, 2-3 m; otherwise poor	No, due to abundance of pebbles, cobbles & boulders; Holocene alluvium; interbedded pebbley sand & silt containing buried soils	No dates	No	Not applicable

		overlying boulders & cobbles			
Eastern Coast and Inland					
Fajardo 5.7 km	Good to excellent in bends along upstream third, 7-8 m high; fewer exposures along down-stream two thirds, 3-4 m high	No, due to paucity of loose sandy sediment; Holocene alluvial and debris avalanche deposits; silt with buried soils overlying pebbles and cobbles	No dates	No	Not applicable
Blanco 10 km	Good to excellent in bends along upstream half, 3 m high; fewer exposures along downstream half, 2 m high	Yes; Holocene alluvium & possibly beach deposits near coast; light brown silt & reddish-brown silt or interbed-ded silt, sandy silt, & fine-medium sand, over-lying sand & pebbley sand at or below base of cutbank; 1-2 buried soils	A.D. 1683 from RB1-C1; wood collected 2.7 m BTC; weathered sediment with buried soils likely older	No	Not applicable
Humacao, in vicinity of city of Humacao 3.2 km	Few exposures, 6-8 m high; otherwise heavily vegetated	Yes, but limited exposure of fluvial deposit; Holocene alluvium & fanglomerate deposits; reddish silt & medium to coarse sand overlying soil developed in clayey sand & clayey silt with granules, pebbles, & cobbles	No dates	No	Not applicable
Maunabo 4.7 km	Good to excellent in occasional bends along upstream section, 4-5 m high; no exposure along lower 0.7 km	Yes; Holocene alluvium overlying Pleistocene alluvium; interbedded silt & sand overlying paleosol developed in reddish clay & pebbley sandy clay	No dates	No	Not applicable
Gurabo 23.6 km	Good to excellent in many river bends, otherwise vegetated; upstream third, 5-10 m high; middle third, 3-8 m high; down-stream third, 3-5	Yes; Holocene alluvium; upstream third: multiple fining upward sequences of pebbley sand, sandy silt, & silt separated by soils; middle third: inter-bedded silt, sand, & pebbley sand with multiple buried soils; lower third: silt with thin	A.D. 412 from RG8-C3, plant material collected ~6 m BTC	No	Not applicable

	m high, fewer exposures	interbeds of sand over-lying crossbedded fine-medium sand			
Grande de Loíza 11.2 km	Few exposures in river bends, 3-5 m high; excellent exposure near pumping station	No; due to prevalence of pebbles and cobbles; Quaternary alluvium, terrace deposits; weathered sand over-lying pebbles & cobbles	No dates	No	Not applicable
Valenciano 2.5 km	Good to excellent in many river bends, 4-6 m high; otherwise heavily vegetated	Yes; Holocene alluvium; interbedded silt, sand, & pebbley sand containing buried soils & channel fill deposits; sand layers exhibited soil lamellae	1369 B.C. from RV3-C1, charred material collected ~4.5 m BTC	No	Not applicable

***** Sediment ages from maximum dates of samples collected from river cutbanks; may not reflect the maximum age of sediment exposed in cutbanks; BTC – below top of cutbank.

INTCAL20 database (Reimer et al., 2020). The results of radiocarbon dating, their conventional ages, recalibrated ages and calendar dates, and material and position descriptions are presented in Table S2 in the Supplement.

The age estimates of all liquefaction features were reviewed and, in some cases, reinterpreted. During this process, radiocarbon dates at the liquefaction sites and/or nearby sites were considered as were the positions of liquefaction features in the cutbank and weathering of the features. Unfortunately, the sedimentary record of exposed sediment is quite limited along several of the rivers. The shortest records occur along Río Blanco and Río Grande de Anasco and are about 0.4 kyr and 0.6 kyr long, respectively (Table 1). The sediment records along Río Culebrinas, Río de la Plata, and Río Gurabo range from 1-1.6 kyr long. The longest records occur along Río Valenciano and Río Grande de Manati and are about 3.4 kyr and 5.4 kyr long, respectively. Sites where there are crosscutting relationships between multiple generations of features are especially important for establishing the number of earthquakes that induced liquefaction along a river. Two generations of liquefaction features that formed in the past 600 years were found along Río Grande de Anasco, three generations of features that formed in the past 1,000 years and 5,400 years were found along Río Culebrinas and Río Grande de Manati, respectively. Information about the liquefaction sites and features, as well as constraining dates and interpreted events are presented in Table S1 in the Supplement.

Several historical earthquakes are known to have induced liquefaction in Puerto Rico. The 1918 earthquake induced liquefaction in Río Grande de Añasco valley and near Río Culebrinas (Moya and McCann, 1991), and the 1670 earthquake induced liquefaction along the Yaquez River near Mayagüez (Moya, 1998). Therefore, liquefaction features found along Río Grande de Añasco (RGA) and Río Culebrinas (RC) that formed during the past 400 years are attributed to these two historical earthquakes (Figures 6 and 7; Figures S1-S5 in the Supplement). These features tend to occur high in the sediment section and are relatively unweathered.

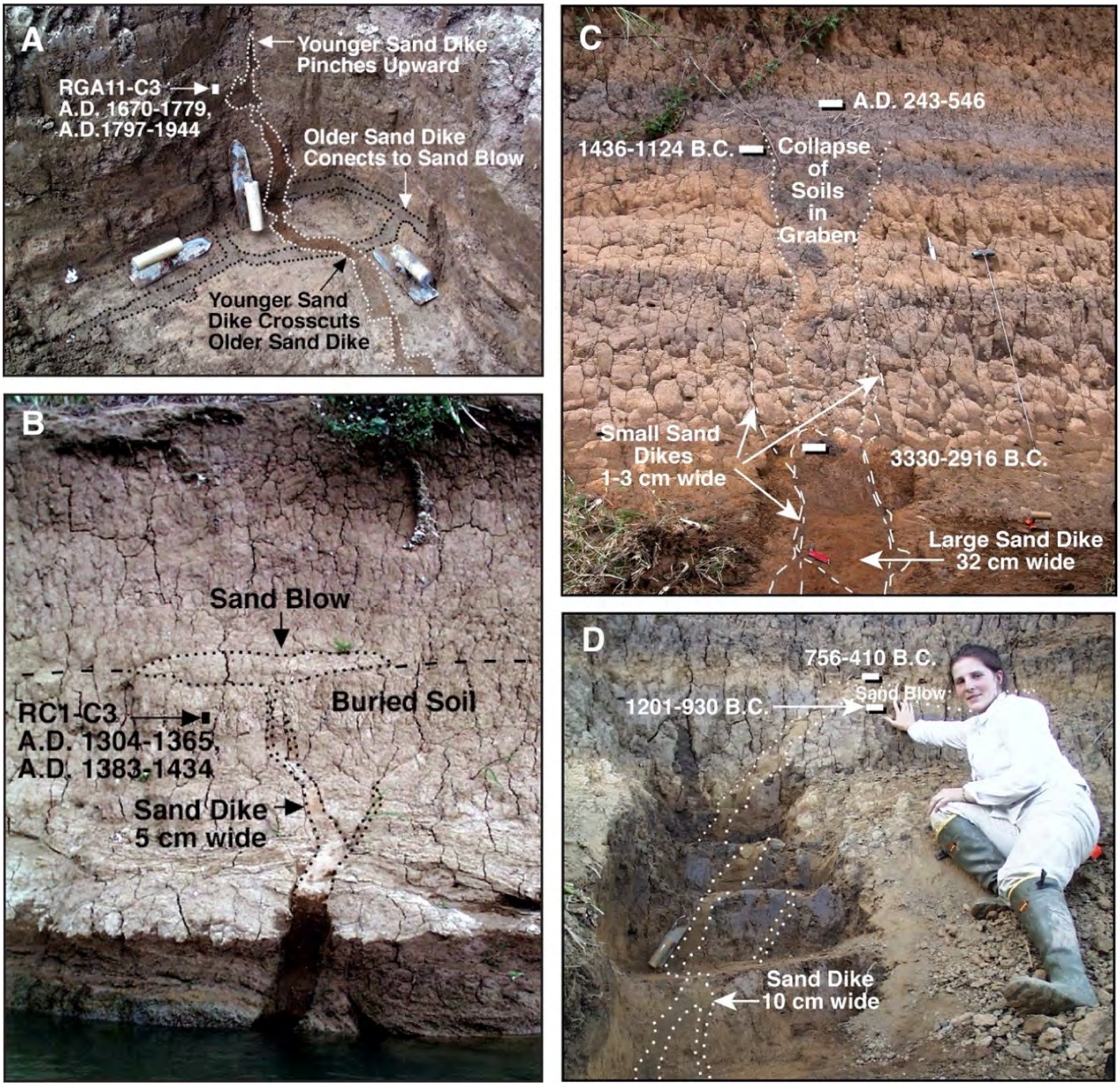

Figure 7. Examples of earthquake-induced liquefaction features: (A) At site RGA11, notice crosscutting relationship between two generations of liquefaction features. On basis of dating of sample RGA11-C5 (not shown) collected below sand blow, both generations of features formed since A.D. 1644, probably during historic earthquakes of 1670 and 1918; (B) at site RC1, sample RC1-C3 of charred material from buried soil crosscut by sand dikes and overlain by sand blow provides close maximum age of A.D. 1304 –1434 for the liquefaction features interpreted to have formed during a large earthquake circa A.D. 1304-1508; (C) at site RGM2N, large sand dike at base of cutbank and related graben fill above formed between 1436 B.C. and A.D. 546 based on dating of disturbed and undisturbed buried soils, respectively; two younger generations of sand dikes crosscut large sand dike and formed during later earthquakes; (D) at site RGM1, upstream from RGM2N, sand dike and related sand blow formed between 1201 B.C and 410 B.C. based on dating of buried soils below and above sand blow, respectively. Additional examples of liquefaction features are shown in Figures S6-S10 in the Supplement.

The 1787 earthquake caused widespread damage across the island except in the south and is thought to have ruptured the Puerto Rico segment of the plate interface (McCann, 1985) or a fault along the northern coast of the island (ten Brink et al., 2011). This event reportedly caused several structures in San Juan to collapse (Hernández, 1985), suggesting shaking intensity, perhaps Modified Mercalli intensity VII-VII, strong enough to induce liquefaction in susceptible sediment along the north coast. Though their ages are poorly constrained, liquefaction features along the Río Grande de Manatí (RGM) that formed during the past 1,000 years and are relatively unweathered are attributed to the 1787 earthquake.

Liquefaction features that formed during prehistorical earthquakes were found on Río Culebrinas, Río Grande de Manatí, and Río de La Plata (Figures 6 and 7, and Figure S1-S5 in the Supplement). Radiocarbon dating at multiple sites are used to estimate the ages of these features that tend to occur lower in the sediment section and are much more weathered than those features attributed to historical earthquakes. Liquefaction features attributed to an earthquake about A.D. 1304-1508 occur along Río Culebrinas, Río Grande de Manatí, and Río de La Plata. Liquefaction features and related ground failure attributed to an earthquake about 1201-410 B.C. occur only on Río Grande de Manatí.

Liquefaction information for Puerto Rico was entered into an EXCEL file, and along with a derivative shapefile, are available online at http://mptuttle.com/databases.html). The information includes locations, types, measured sizes, maximum and minimum radiocarbon ages, age estimates, weathering characteristics, location of geotechnical data, references, and comments. Also, radiocarbon data was entered into an EXCEL spreadsheet and is available online at http://mptuttle.com/databases.html). This report along with GIS-based maps illustrating the ages, sizes, and locations of liquefaction features for the island and for each river valley where features were found (Río Grande de Añasco, Río Culebrinas, Río Guanajibo, Río Grande de Manatí, and Río de La Plata) are available online at http://mptuttle.com/projects.html).

Evaluation of Scenario Earthquakes

During previous studies, scenario earthquakes were evaluated to determine whether or not they would be likely to induce liquefaction along the surveyed rivers and those results were compared with observations of liquefaction in the field. Although the cyclic stress method used in liquefaction potential analysis (e.g., Seed and Idriss, 1971; Youd and Idriss, 2003) has changed little in the past ten years, there have been significant changes in ground motion prediction equations (GMPEs) that are used to calculate peak ground accelerations of the scenario earthquakes. Therefore, we reevaluated scenario earthquakes using the updated GMPEs developed during the NGA-West2 project (e.g., Seyhan, 2015). A review of liquefaction potential analysis used in the evaluation of scenario earthquakes is provided in the Supplement.

Geotechnical data used in the liquefaction potential analysis were gleaned from borehole logs provided by Puerto Rico Department of Transportation and Public Works. The borehole logs were collected at bridge crossings of the Río Grande de Añasco, Río Culebrinas, Río Guanajibo, Río Grande de Manatí, Río de la Plata, Río Blanco, and Rio Gurabo near the confluence with Rio Valenciano. The borehole locations are shown on Figure 5 and Figures S1-S5 in the Supplement. The borehole logs were reviewed and layers susceptible to liquefaction selected for liquefaction potential analysis. These include sandy layers less than 16 m below the surface, likely to be below

the water-table at least part of the year, and characterized by blow counts (N, a measure of soil density) of less than 30. The selected layers and their characteristics are summarized in Table S3 of the Supplement. Distances between the scenario earthquakes and borehole locations was needed to calculate peak ground accelerations of the scenario earthquakes. The distances were measured within the GIS framework and are shown in Tables S4-S15. Analysis was performed for two water table depths, 1 m and 3 m, in order to capture fluctuations in the water table over time.

Scenario earthquakes were evaluated for the historical earthquakes of 1918, 1787, and 1670 and for the paleoearthquakes in A.D. 1304-1508 and 1201-410 B.C. interpreted from liquefaction features. In addition, a paleoearthquake in A.D. 1200-1480 interpreted from tsunami deposits (e.g., Atwater et al., 2017; Fuentes et al., 2017; Tuttle and Fuentes, 2021; Biguenet et al., 2021; Cordrie et al., 2022) also was evaluated. Given the similarity in timing, the A.D. 1304-1508 and A.D. 1200-1480 events might represent the same earthquake or a cluster of earthquakes resulting from multiple ruptures of the North America-Caribbean plate interface or outer-rise normal faults. A list of the scenario earthquakes is provided in Table 2 and the locations of the scenario earthquakes are shown on Figure 8.

Scenario earthquakes evaluated using liquefaction potential analysis include the following:

- For the 1918 event with the location given in the ANSS catalog (U.S. Geological Survey, 2017) and thought to be due to Mona Canyon normal faulting, **M** 7.1 and 7.7 earthquakes;
- For the 1787 event with the location provided in the U.S. Geological Survey catalog (Mueller et al., 2003) and thought to have been produced by the plate interface, **M** 7.7 and 8.0 earthquakes; and alternatively, with location 2 of ten Brink et al. (2011) along the north coast of the island, **M** 6.4 earthquake;
- The magnitude and location of the 1670 earthquake are essentially unknown; therefore, scenario earthquakes of **M** 6.0-6.7 with three locations associated with mapped faults in western Puerto Rico;
- For the A.D. 1304-1508 event, **M** 8.0-8.5 earthquakes with two locations: A along the North America-Caribbean plate interface north of Mona Canyon; B along the eastern Septentrional fault zone and in the gap between the rupture zones of the 1943 and 1946 earthquakes (Dolan and Wald, 1998; Doser et al., 2005); also, **M** 8.0 and 8.25 earthquakes with location C along the Bowin fault, a possible eastward extension of the Septentrional fault and north of a large submarine slump scarp off the north-central coast of Puerto Rico (Grindlay et al., 2005a; Mercado et al., 2020);
- For the A.D. 1200-1480 event, a **M** 8.45 earthquake with the westernmost location of a multi-segment rupture (CDE) of the plate interface as proposed by Wei (2022);
- For the 1201-410 B.C. event, **M** 8.0 and 8.5 earthquakes with a location C along the Bowin fault zone and **M** 6.2 with a location D along the GNPRFZ.

M 8.5 is the largest magnitude evaluated since that is the maximum magnitude for which the validation tool used in this study is applicable. The results of liquefaction potential analysis for the scenario earthquakes are summarized in Tables 3-6 and provided in more detail in Tables S4-S15 in the Supplement.

Table 2. Scenario earthquakes used in liquefaction potential analysis.

Event	Possible Source (Fig. 8 ID)	Latitude (°N)	Longitude (°W)	Moment Magnitude	Information on Sources
A.D 1918	Mona Canyon normal faulting	18.8020	-67.2190	7.1, 7.4	ANSS catalog (U.S. Geological Survey, 2017; Grindlay et al., 1997; van Gestel et al., 1998; Doser et al., 2005)
A.D. 1787	Plate interface north of Puerto Rico	19.0000	-66.0000	7.7, 8.0	USGS catalog (McCann, 1985; Mueller et al., 2003 & 2010)
A.D. 1787	North coast of Puerto Rico (ten Brink et al., 2011)	18.2500	-66.5000	6.4	Ten Brink et al., 2011 (location 2)
A.D. 1670	Cerro Godin fault zone	18.3422	-67.1419	6.0, 6.2	This paper (McIntyre, 1971; Mann et al., 2005)
A.D. 1670	Mayaguez	18.1792	-67.0445	6.0, 6.5	This paper (Glover, 1971; Moya, 1998; Grindlay at el., 2005c)
A.D. 1670	So. Lajas fault	18.0269	-67.1275	6.7	This paper (Prentice & Mann, 2005)
A.D. 1304-1508	Plate interface north of Mona Canyon (A)	19.1031	-67.3932	8.0, 8.5	This paper (Wei, 2022)
A.D. 1304-1508	Eastern Septentrional fault zone (B)	19.0041	-68.0791	8.0, 8.5	This paper (LaForge & McCann, 2005; Dolan and Wald, 1998; Doser et al., 2005; Wei, 2022)
A.D. 1304-1508	Bowin fault zone north of Puerto Rico (C)	19.1926	-66.6779	8.0, 8.25	This paper (Grindlay et al., 1997 & 2005b; LaForge & McCann, 2005)
A.D. 1200-1480	Plate interface northeast of Puerto Rico	19.0711	-64.9574	8.45	Wei et al., 2016; Atwater et al., 2017; Fuentes et al., 2017; Wei, 2022
1201-410 B.C.	Bowin fault zone north of Puerto Rico (C)	19.1926	-66.6779	7.6	This paper (Grindlay et al., 1997 & 2005b; LaForge & McCann, 2005)
1201-410 B.C.	GNPRFZ south of Manati (D)	18.2500	-66.5000	6.2	This paper (Briggs, 1964; Geomatrix, 1988)

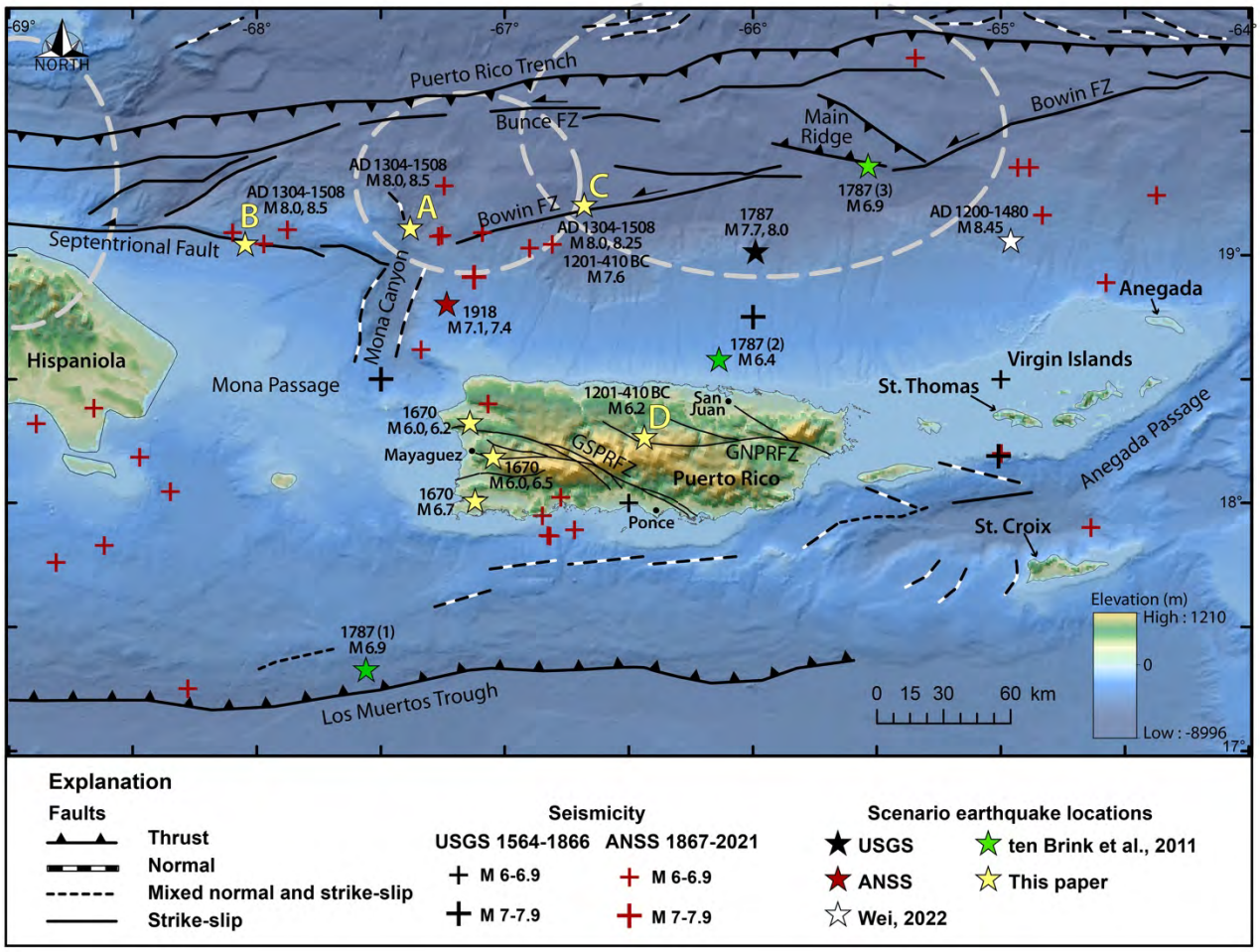

Figure 8. Regional map showing locations and magnitudes of scenario earthquakes (indicated by stars) evaluated using liquefaction potential analysis. Of three possible magnitudes and locations proposed by ten Brink et al. (2011) for 1787 earthquake, only location 2 is evaluated since other two alternatives are unlikely to induce liquefaction on the island. Dashed white lines represent approximate rupture areas of historic earthquakes (left to right - 1946, 1943, and 1787 after McCann, 1985; Dolan and Wald, 1998; Doser et al., 2005).

The 1918 Earthquake

As mentioned earlier, liquefaction features thought to have formed as a result of the 1918 earthquake occur on Río Grande de Añasco, Río Culebrinas, and possibly Río Guanijibo, with the largest features, including sand blows, on Río Culebrinas (Figure 6). The **M** 7.4 scenario earthquake provides the best match between predicted and observed liquefaction (Table 3). Analysis of the **M** 7.1 scenario earthquake predicts liquefaction only along the Río Grande de Añasco. According to the analysis, neither scenario earthquake predicts liquefaction along Río Grande de Manatí or Río de la Plata which matches field observations.

According to the ISC-GEM catalog on which the magnitude in the ANSS catalog is based, the 1918 earthquake was of **M** 7.1 +/- 0.30. Therefore, a **M** 7.4 is within the magnitude uncertainty range for this event, and liquefaction potential analysis using the updated GMPEs seems

applicable in this setting. Some researchers place the 1918 earthquake southwest of the ANSS location (e.g., Doser et al., 2005). If the event were located closer to northwestern Puerto Rico, the magnitude required to induce liquefaction along the western rivers would be lower.

Table 3. Results summary of liquefaction potential analysis for scenarios of A.D. 1918 and A.D. 1787 earthquakes.

Rivers	AD 1918 Mona Passage M 7.1	AD 1918 Mona Passage M 7.4†	AD 1787 USGS M 7.7†	AD 1787 USGS M 8.0	AD 1787 ten Brink (2) M 6.4
Culebrinas	N, N	L, N	N, N	N, N	N, N
Grande de Añasco	L, N L/N, N	L, L L, L/N	N, N N, N	N, N N, N	N, N N, N
Guanajibo	N, N	L, N	NA	NA	NA
Grande de Manati	N, N	N, N	L, L	L, L	N, N
de la Plata	N, N N, N	N, N N, N	N, N N, N	L, N L/N, N	N, N N, N
Gurabo	NA	NA	L/N, N	L, L/N	N, N
Blanco	NA	NA	N, N	L/N, L/N	N, N

† Gray shading indicates preferred scenario earthquake; dark gray shading indicates observed liquefaction.

L = Liquefaction likely for 45% - 100% of the layers analyzed; L/N = marginal because liquefaction predicted for 24% - 44% of the layers analyzed; N = liquefaction not likely because liquefaction predicted for less than 24% of the layers analyzed. Two results per location reflect results for water table depths, 1 m and 3 m, respectively.

NA – liquefaction potential analysis has not yet been performed for this location; liquefaction unlikely due to distance from source.

The 1787 Earthquake

Liquefaction features, including sand dikes and sills, attributed to the 1787 earthquake occur only along Río Grande de Manatí (Figure 6). The **M** 7.7 scenario earthquake with the USGS location provides the best match between predicted and observed liquefaction (Table 3). According to the analysis, such an earthquake would be likely to induce liquefaction along Río Grande de Añasco and could produce marginal liquefaction along Río Gurabo. Given that marginal liquefaction occurs in a low percentage of sandy layers, it would not be surprising not to find liquefaction features under these circumstances. The **M** 8.0 scenario earthquake with the USGS location would likely induce liquefaction along Río Grande de Manati, Río de la Plata, and rivers in eastern Puerto Rico, including Río Blanco as well as Río Gurabo. In contrast, the **M** 6.4 scenario earthquake with a proposed location along the northern coast (Brink et al., 2011) would not induce liquefaction along Río Grande de Manati or any of the other rivers included in the analysis.

The 1670 Earthquake

Liquefaction features attributed to the 1670 earthquake occur along Río Grande de Añasco, Río Culebrinas, and possibly Río Guanijibo, with the largest features, including sand blows, along

Río Grande de Añasco (Figure 6). Previously, liquefaction features attributed to the A.D. 1670 earthquake had been found at an archeological site east of Mayagüez along the Yaquez River (Moya, 1998). The **M** 6.2 scenario earthquake located on the Cerro Godin fault zone north of Río Grande de Añasco provides the best match between predicted and observed liquefaction (Table 4). The next best fit is the **M** 6.0 scenario earthquake located on the Cerro Godin fault zone but it produces only marginal liquefaction along the Río Culebrinas. The **M** 6.0 scenario earthquake located east of Mayaguez and the **M** 6.5 and **M** 6.7 scenario earthquakes along the South Lajas fault do not predict liquefaction along Río Culebrinas.

Table 4. Results summary of liquefaction potential analysis for scenarios of A.D. 1670 earthquake.

Rivers	AD 1670 Cerro Godin M 6.0	AD 1670 Cerro Godin M 6.2†	AD 1670 Mayaguez M 6.0	AD 1670 Mayaguez M 6.5	AD 1670 So. Lajas M 6.7
Culebrinas	L/N, N	L, L	N, N	N, N	N, N
Grande de Añasco	L, L L, L	L, L L, L	L, L L, L/N	L, L L, L	L, L L, L/N
Guanajibo	L, L	L, L	L, L	L, L	L, L
Grande de Manati	N, N	N, N	N, N	N, N	N, N
de la Plata	NA	NA	NA	NA	NA
Gurabo	NA	NA	NA	NA	NA
Blanco	NA	NA	NA	NA	NA

† Gray shading indicates preferred scenario earthquake; dark gray shading indicates observed liquefaction.

L = Liquefaction likely for 45% - 100% of the layers analyzed; L/N = marginal because liquefaction predicted for 24% - 44% of the layers analyzed; N = liquefaction not likely because liquefaction predicted for less than 24% of the layers analyzed. Two results per location reflect results for water table depths, 1 m and 3 m, respectively.

NA – liquefaction potential analysis has not yet been performed for this location; liquefaction unlikely due to distance from source.

The A.D. 1304-1508 Earthquake

Liquefaction features thought to have formed during a paleoearthquake in A.D. 1304-1508 occur along Río Culebrinas, Río Grande de Manatí, and Río de la Plata, with the largest features including a sand blow along Río Culebrinas (Figure 6). Scenario earthquakes of **M** 8.0 and **M** 8.5 were evaluated at two different locations (A and B) along the plate interface and the eastern Septentrional fault zone (Table 5). Also, **M** 8.0 and **M** 8.25 scenario earthquakes were evaluated at a third location along the Bowin fault zone (C) (Table 6).

Of all the scenario earthquakes considered, the **M** 8.5 at location B on the eastern Septentrional fault zone seems the best match. The **M** 8.0 scenario earthquakes at locations A and B underpredict liquefaction along all three rivers (Table 5); whereas, the **M** 8.5 events at locations A and B predict liquefaction along Río Culebrinas and Río Grande de Manatí, but not along Río de la Plata. Larger magnitude scenario earthquakes would predict liquefaction along Río de la Plata, but analyzing a **M** >8.5 event is beyond the applicability of the validation tool used in this

study. Of the two **M** 8.5 scenario earthquakes, the one at location B is preferred because it predicts liquefaction for both water-table depths at Río Culebrinas and for only the shallow water-table depth for Río Grande de Manatí, suggesting more significant liquefaction along Río Culebrinas than Río Grande de Manati.

Interestingly, location B is in the gap between the 1943 and 1946 rupture zones and where no large earthquake has relieved stress during the historical period (Figure 8; Doser et al., 2005). Liquefaction features, including sand dikes and compound sand blows, formed in the eastern Cibao valley of the Dominican Republic (DR) during large earthquakes between A.D. 1060 and A.D. 1492 (Tuttle et al., 2003). The features were interpreted to have formed during a sequence of earthquakes resulting from ruptures of the Septentrional fault zone in central and eastern DR. However, a **M** 8.5 earthquake at location B on the eastern Septentrional fault zone could induce liquefaction in susceptible sediment 185-195 km away, the distance to liquefaction features in the eastern Cibao valley, according to the earthquake magnitude-liquefaction distance relationship (e.g., Ambraseys, 1988; Castilla and Audemard, 2007). Improved age estimates of liquefaction features and additional liquefaction potential analysis are needed to test the hypothesis that a **M** 8.5 earthquake at location B induced liquefaction in the Cibao valley in A.D. 1304-1508.

Table 5. Results summary of liquefaction potential analysis for scenarios of A.D. 1304-1508 earthquake with North America plate interface (NAPI) and eastern Septentrional fault zone (ES) as sources.

Rivers	AD 1304-1508 NAPI (A) M 8.0	AD 1304-1508 NAPI (A) M 8.5	AD 1304-1508 ES (B) M 8.0	AD 1304-1508 ES (B) M 8.5	AD 1200-1480 NAPI (Wei) M 8.45
Culebrinas	L, N	L, L	N, N	L, L	NA
Grande de Añasco	L, L L, L/N	L, L L, L	L, N L, L/N	L, L L, L	NA
Guanajibo	NA	NA	NA	NA	NA
Grande de Manati	L, L/N	L, L	N, N	L, N	L/N, N
de la Plata	N, N N, N	N, N N, N	N, N N, N	N, N N, N	N, N N, N
Gurabo	N, N	N, N	N, N	N, N	L/N, N
Blanco	N, N	N, N	N, N	N, N	L/N, L/N

† Gray shading indicates preferred scenario earthquake; dark gray shading indicates observed liquefaction.

L = Liquefaction likely for 45% - 100% of the layers analyzed; L/N = marginal because liquefaction predicted for 24% - 44% of the layers analyzed; N = liquefaction not likely because liquefaction predicted for less than 24% of the layers analyzed. Two results per location reflect results for water table depths, 1 m and 3 m, respectively.

NA – liquefaction potential analysis has not yet been performed for this location; liquefaction unlikely due to distance from source.

At location C along the Bowin fault, the **M** 8.0 scenario earthquake predicts liquefaction at Río Grande de Manatí, but not at Río Culebrinas nor at Río de la Plata (Table 6). The **M** 8.25 scenario earthquake at location C predicts liquefaction along Río Grande de Manatí, liquefaction along Río Culebrinas and Río de la Plata but only during shallow water-table conditions, and

marginal liquefaction along Río Gurabo. Both scenario events at location C, underpredict liquefaction along Río Culebrinas attributed to a paleoearthquake in A.D. 1304-1508.

Table 6. Results summary of liquefaction potential analysis for scenarios of A.D. 1304-1508 and 1201-410 B.C. earthquakes.

Rivers	AD 1304-1508 Bowin Fault (C) M 8.0	AD 1304-1508 Bowin Fault (C) M 8.25†	1201-410 BC Bowin Fault (C) M 7.6	1201-410 BC Bowin Fault (C) M 7.8†	1201-410 BC GNPRFZ (D) M 6.2
Culebrinas	N, N	L, N	N, N	N, N	N, N
Grande de Añasco	L, L L/N, N	L, L L, L	N, N N, N	L, N N, N	N, N N, N
Guanajibo	NA	NA	N, N	N, N	N, N
Grande de Manati	L, L	L, L	L, N	L, L	L, L/N
de la Plata	N, N N, N	L, N N, N	N, N N, N	N, N N, N	N, N N, N
Gurabo	N, N	L/N, N	N, N	N, N	N, N
Blanco	N, N	N, N	N, N	N, N	N, N

† Gray shading indicates preferred scenario earthquake; dark gray shading indicates observed liquefaction.

L = Liquefaction likely for 45% - 100% of the layers analyzed; L/N = marginal because liquefaction predicted for 24% - 44% of the layers analyzed; N = liquefaction not likely because liquefaction predicted for less than 24% of the layers analyzed. Two results per location reflect results for water table depths, 1 m and 3 m, respectively.

NA – liquefaction potential analysis has not yet been performed for this location; liquefaction unlikely due to distance from source.

The A.D. 1200-1480 Earthquake

The scenario earthquake of **M** 8.45 located northwest of Anegada (Figure 8; Wei, 2022) predicts marginal liquefaction at Río Grande de Manatí, Río Blanco, and Río Gurabo (Table 5), suggesting that the A.D. 1200-1480 earthquake, responsible for tsunami deposits on Anegada and St. Thomas, is not the earthquake responsible for liquefaction features and tsunami deposits on Puerto Rico that formed in A.D. 1304-1508. This would be consistent with the hypothesis that tsunami deposits discovered on several islands in the northeastern Caribbean are the result of a cluster of **M** 8-9 earthquakes resulting from ruptures of the North America-Caribbean plate interface or outer-rise normal faults between A.D. 1200-1500 (Cordrie et al., 2022).

The 1201-410 B.C. Earthquake

Liquefaction features thought to have formed during a paleoearthquake in 1201-410 B.C. were found only along Río Grande de Manatí, though this may be an underrepresentation of liquefaction induced by the event given the limited age of sediment exposed along many of the rivers. The features on the Río Grande de Manatí that formed during the 1201-410 B.C. event include the largest sand blow and sand dikes documented along all of the rivers (Figure 7C). Also, they are larger than younger features along the Manatí, suggesting stronger ground motions along this river during the 1201-410 B.C. event than during the A.D. 1304-1508 and A.D. 1787

events. The large size of the oldest features suggests an earthquake source relatively close to Río Grande de Manatí. Therefore, the Bowin fault zone and the onshore GNPRFZ were considered as earthquake sources.

Scenario earthquakes of **M** 7.6 and **M** 7.8 were evaluated at location C along the Bowin fault. Both scenarios forecast liquefaction along Río Grande de Manatí but the **M** 7.8 event is preferred because it predicts liquefaction for both water-table depths and thus more significant liquefaction in line with observations (Table 6 and Table S14). According to the analysis for location D on the GNPRFZ, **M** 6.2 is the smallest scenario earthquake that predicts liquefaction along Río Grande de Manatí (Table 6 and Table S15). Of the two sources, the Bowin fault zone is preferred because tsunami deposits of similar age in northwestern Puerto Rico suggest an offshore source (Figure 4).

Implication of Paleoliquefaction Results for Recurrence Estimates

There is considerable uncertainty about the slip rate and maximum magnitude of the eastern Septentrional fault zone and its possible eastward extension, the Bowin fault zone. For the eastern Septentrional fault, estimates of slip rates range from 2 mm/yr to 9 mm/yr and estimates of maximum magnitude range from **M** 7.3-8.0 (Prentice et al., 2003b; LaForge and McCann, 2005). In the 2003 seismic hazard assessment for Puerto Rico, six rupture scenarios were evaluated to test the plausibility of the slip rates and magnitude estimates (Mueller et al., 2003 and 2010). Recurrence times were found to be too short for high-slip rate (9 mm/yr and 5 mm/yr) **M** 7.3 rupture scenarios, given that no very large earthquakes have been associated with the eastern Septentrional fault zone during the historical period. The remaining scenarios included recurrence times of 310 years for **M** 7.3 earthquakes and 770-3600 years for **M** 8.0 earthquakes. The finding of this paleoliquefaction study, that a **M** 8.5 may have occurred on the eastern Septentrional fault zone circa A.D. 1304-1508, suggests that the recurrence time for great earthquakes on this fault is at least 514-718 years and possibly much longer.

For the Bowin fault zone, estimates of the slip rate range from 0 mm/yr to 9 mm/yr and a maximum magnitude of **M** 7.6 is derived from its length of ~160 km (LaForge and McCann, 2005; Wells and Coppersmith, 1994). In the 2003 seismic hazard assessment, a slip rate of 1 mm/yr, corresponding to a recurrence time of 3,900 years, was assigned to the Bowin fault zone. In this paleoliquefaction study, it was found that a **M** 7.8 produced by the Bowin fault zone circa 1201-410 B.C. may have been responsible for liquefaction and ground failure on the Río Grande de Manatí. If so, the finding suggests a recurrence time of at least 2432-3223 years for very large earthquakes on the Bowin fault.

Summary of Findings

Between 2000 and 2011, surveys for earthquake-induced liquefaction features were conducted along all major rivers in western, northern, and eastern Puerto Rico. Surveys were not conducted along rivers in southern Puerto Rico primarily due to scarcity of cutbank exposures in sandy sediment. Sedimentary conditions were found to be suitable for the formation of liquefaction features along most of the rivers surveyed, but the record of past earthquakes is limited by the age of exposed sediment.

More than ninety liquefaction features, including sand dikes, sand blows, and sand sills, were discovered along Río Grande de Anasco, Río Culebrinas, and Río Guanijibo in western Puerto Rico and along Río Grande de Manati and Río de la Plata in north-central Puerto Rico. No liquefaction features were found in northeast and eastern Puerto Rico. Two generations of features along Río Grande de Anasco formed during the past 600 years; three generations of features along Río Culebrinas and Río Grande de Manatí formed during the past 1,000 years and 5,400 years, respectively; and one generation of liquefaction features on Río de la Plata formed during the past 1600 years.

Ages of liquefaction features are estimated on the basis of radiocarbon dating, crosscutting relationships, stratigraphic position, and weathering. Some of the liquefaction features are attributed to the historical earthquakes in 1918 and 1670 known to have induced liquefaction in the vicinity of Río Grande de Anasco and Río Culebrinas or to the historical earthquake of 1787 which caused shaking along the north-central coast strong enough to induce liquefaction. Age estimates of other liquefaction features indicate that they formed about A.D. 1304-1508 and 1201-410 B.C.

Sand dikes and sand blows attributed to the 1918 earthquake and/or the A.D. 1670 earthquake occur on Río Grande de Añasco, Río Culebrinas, and possibly Río Guanijibo. Sand dikes and a sill attributed to the A.D. 1787 earthquake occur only along Río Grande de Manatí. Liquefaction features thought to have formed during a paleoearthquake in A.D. 1304-1508 occur along Río Culebrinas, Río Grande de Manatí, and Río de la Plata, with the largest sand blow and sand dikes for this event on Río Culebrinas. Liquefaction features thought to have formed during a paleoearthquake in 1201-410 B.C. were found only along Río Grande de Manatí. They include the largest sand blow and sand dikes documented along all of the rivers and are larger than younger features along the Manatí.

Scenario earthquakes representing various magnitudes and source locations were evaluated using liquefaction potential analysis. The ANSS catalog location was used for the 1918 earthquake; the USGS catalog locations and an alternate location proposed by ten Brink et al. (2011) were used for the 1787 earthquake. On the basis of the evaluation, scenario earthquakes that would most likely produce liquefaction observed in the field are as follows:

- 1918 earthquake - **M** 7.4 associated with Mona Passage normal faults;
- 1787 earthquake - **M** 7.7 associated with plate interface north of Puerto Rico;
- 1670 earthquake - **M** 6.2 located on the Cerro Godin fault zone north of Añasco;
- A.D. 1304-1508 paleoearthquake - **M** 8.5 associated with the eastern Septentrional fault zone;
- A.D. 1200-1480 paleoearthquake - **M** 8.45 located northeast of Puerto Rico unlikely to be responsible for liquefaction features on Puerto Rico that formed in A.D. 1304-1508;
- 1201-410 B.C. paleoearthquake - **M** 7.8 associated with the Bowin fault zone.

There is considerable uncertainty about the slip rate, maximum magnitude, and recurrence times of the eastern Septentrional and Bowin fault zones. This paleoliquefaction study finds that a **M** 8.5 earthquake may have occurred on the eastern Septentrional fault zone circa A.D. 1304-1508 and a **M** 7.8 earthquake may have occurred on the Bowin fault zone circa 1201-410 B.C. If so, the recurrence time is at least 514-718 years and possibly much longer for great earthquakes on

the eastern Septentrional fault zone, and at least 2,432-3,223 years for very large earthquakes on the Bowin fault zone. This new information about paleoearthquakes in A.D. 1304-1508 and 1201-410 B.C., their likely magnitudes and source locations, and minimum recurrence times of large earthquakes on those sources may contribute to the update of the seismic source model and help to reduce uncertainties in the seismic hazard assessment for the PRVI region.

Conclusions

On the basis of field observations of liquefaction features along rivers in western and north-central Puerto Rico, age estimates of those liquefaction features, and evaluation of scenario earthquakes using liquefaction potential analysis, the main conclusions of this study are as follows:

- The 1918 earthquake may have been of **M** 7.4 if it had a location similar to that given in the ANSS catalog; the 1787 earthquake may have been of **M** 7.7 if it had the location similar to that given in the USGS catalog; and the 1670 earthquake may have been about **M** 6.2 and located near Añasco.

- A paleoearthquake circa A.D. 1304-1508 induced liquefaction in northwestern and north-central Puerto Rico; and a paleoearthquake circa 1201-410 B.C. induced liquefaction in north-central Puerto Rico.

- The paleoearthquake in A.D. 1304-1508 may have been of **M** 8.5 and produced by the eastern Septentrional fault zone, where there have been no major earthquakes during the historical period. If so, it suggests a recurrence time of at least 514 years, and possibly much longer, for great earthquakes on the eastern Septentrional fault zone.

- The paleoearthquakes in 1201-410 B.C. may have been of **M** 7.8 and produced by the Bowin fault zone, not far from a large submarine slump scarp off the north-central coast of Puerto Rico. If so, this finding suggests a recurrence time of at least 2,432 years for very large earthquakes on the Bowin fault zone.

Data and Resources

Bathymetry for regional maps:
GEBCO Compilation Group (2022) GEBCO_2022 Grid (doi:10.5285/e0f0bb80-ab44-2739-e053-6c86abc0289c).

Earthquakes 1867-2021:
U.S. Geological Survey, Earthquake Hazards Program, 2017, Advanced National Seismic System (ANSS) Comprehensive Catalog of Earthquake Events and Products: Various, https://doi.org/10.5066/F7MS3QZH.

Earthquakes 1564-1866:
Mueller, C. S., A. D. Frankel, M. D. Petersen, and E. V. Leyendecker, 2003, Documentation for 2003 USGS seismic hazard maps of Puerto Rico and the U.S. Virgin Islands, USGS, Golden, Colorado, http://eqhazmaps.usgs.gov/html/prvi2003.html.

Digital Elevation Models for regional maps:
Amante, Christopher. ETOPO1 1 Arc-Minute Global Relief Model: Procedures, Data Sources and Analysis, Boulder, Colorado: U.S. Dept. of Commerce, National Oceanic and Atmospheric Administration, National Environmental Satellite, Data, and Information Service, National Geophysical Data Center, Marine Geology and Geophysics Division, 2009.

Digital Elevation Models for Puerto Rico island map:
U.S. Geological Survey, 2019, 3D Elevation Program 1/3 Arc-Second Resolution Digital Elevation Model (published 20200606), accessed July 10, 2020 at URL https://apps.nationalmap.gov/downloader/#/.

Digital Elevation Models for maps of Puerto Rico river valleys:
U.S. Geological Survey, 2019, 3D Elevation Program 1-Meter Resolution Digital Elevation Model (published 20200606), accessed August 22, 2021 at URL https://apps.nationalmap.gov/downloader/#/.

Quaternary alluvium:
Bawiec, W. J., editor, 1999, Geology, geochemistry, geophysics, mineral occurrences and mineral resource assessment for the Commonwealth of Puerto Rico, U.S. Geological Survey Open-File Report 98-038, https://pubs.usgs.gov/of/1998/of98-038/.

Acknowledgment of Support and Disclaimer

Material presented in this report is based upon research supported by the U.S. Geological Survey under Grant No. G21AP10006. The views and conclusions contained in this document are those of the authors and should not be interpreted as representing the opinions or policies, either expressed or implied, of the U.S. Geological Survey. Mention of trade names or commercial products does not constitute their endorsement by the U.S. Geological Survey.

References Cited

Ambraseys, N. N., 1988, Engineering Seismology: earthquake engineering and structural dynamics, Journal of the International Association of Earthquake Engineering, v. 17, p. 1-105.

Allstadt, K. E., E. M. Thompson, D. Bayouth García, E. Irizarry Brugman, K. Stephen Hughes, and R. G. Schmitt, 2022, Ground failure triggered by the 7 January 2020 M 6.4 Puerto Rico earthquake, Seismological Research Letters, v. 93(2A), p. 594-608, doi: 10.1785/0220210235.

Asencio, E., 1980, Western Puerto Rico seismicity, USGS Open-File Report 80-192, 135 p.

Atlantic and Gulf of Mexico Tsunami Hazard Assessment Group, 2008, Evaluation of Tsunami Sources with the Potential to Impact the U.S. Atlantic and Gulf Coasts - A report to the Nuclear Regulatory Commission: U.S. Geological Survey Administrative Report, 322 p.

Atwater, B. F., ten Brink, U. S., Buckley, M., Halley, R. S., Jaffe, B. E., López-Venagas, A. M., Reinhardt, E. G., Tuttle, M. P., Watt, S., and Wei, Y., 2011, Geomorphic and stratigraphic evidence for a catastrophic tsunami or storm a few centuries ago at Anegada, British Virgin Islands, Natural Hazards, 13 p. and electronic supplement, DOI 10.1007/s11069-010-9622-6.

Atwater, B. F., U. S. ten Brink, A. L. Cescon, N. Feuillet, Z. Fuentes, R. B. Halley, C. Nuñez, E. G. Reinhardt, J. H. Roger, Y. Sawai, M. Spiske, M. P. Tuttle, Y. Wei, and J. Weil-Accardo, 2017, Extreme waves in the British Virgin Islands during the last centuries before 1500 CE, Geosphere, v. 13, n. 2, p. 301–368.

Bawiec, W. J., editor, 1999, Geology, geochemistry, geophysics, mineral occurrences and mineral resource assessment for the Commonwealth of Puerto Rico, U.S. Geological Survey Open-File Report 98-038, https://pubs.usgs.gov/of/1998/of98-038/.

Biguenet, M., P. Sabatier, E. Chaumillon, C. Chague, F. Arnaud, F. Jorissen, T. Coulombier, E. Geba, L. Cordrie, P. Vacher, A. L. Develle, E. Chalmin, F. Soufi, and N. Feuillet, 2021, A 1600 year-long sedimentary record of tsunamis and hurricanes in the Lesser Antilles (Scrub Island Anguilla), Sedimentary Geology, 105806. ISSN 0037-0738. https://doi.org/10.1016/j.sedgeo.2020.105806.

Briggs, R. P., 1964, Provisional geologic map of Puerto Rico and adjacent islands, USGS Miscellaneous Investigations Map I-392, scale 1:240,000.

Bronk Ramsey, C., 2009, Bayesian analysis of radiocarbon dates, Radiocarbon, v. 51, n. 1, p. 337-360.

Castilla, R. A., and F. A. Audemard, 2007, Sand blows as a potential tool for magnitude estimation of pre-instrumental earthquakes, Journal of Seismology, v. 11, p. 473-487.

Cordrie, L., N. Feuillet, A. Gailler, M. Biguenet, E. Chaumillon, and P. Sabatier, 2022, A Megathrust earthquake as source of a Pre-Colombian tsunami in Lesser Antilles: Insight from sediment deposits and tsunami modeling, Earth-Science Reviews, v. 228.

Dolan, J. F., and D. J. Wald, 1998, The 1943–1953 north-central Caribbean earthquakes: Active tectonic setting, seismic hazards, and implications for Caribbean—North America plate motions, *in* Dolan, J. F., and P. Mann, eds., Active strike-slip and collisional tectonics in the northern Caribbean plate collisional zone, Geological Society of America Special Paper 326, p. 143–169.

Doser, D. I., C. M. Rodriguez, and C. Florez, 2005, Historical earthquakes of the Puerto Rico—Virgin Islands region (1915–1963), *in* Mann, P., ed., Active Tectonics and Seismic Hazards of Puerto Rico, the Virgin Islands, and Offshore Areas, Geological Society of America Special Paper 385, p. 103–114.

Fiegel, G.L. and B. L. Kutter, 1994, Liquefaction mechanism for layered soils, Journal of Geotechnical Engineering, v. 120, p. 737–755. doi:10.1061/(ASCE)0733-9410(1994)120:4(737)

Flores, C. H., U. ten Brink, and W. H. Bakun, 2012, Accounts of damage from historical earthquakes in the northeastern Caribbean, to aid in the determination of their location and intensity magnitudes, USGS Open-File Report 2011-1133, 199 p.

Fuentes, Z., M. Tuttle, and W. Schmidt, 2017, Sand scripts of past tsunamis in coastal ponds of St. Thomas, U.S. Virgin Islands, Seismological Research Letters, doi: 10.1785/0220170038.

Geomatrix, 1988, Earthquake ground motions for the Portugues Dam, Puerto Rico, Geological-seismological evaluation to assess potential hazards, Department of the Army, Jacksonville District, Corps of Engineers, Jacksonville, Florida, 83 p., plus Appendices.

Glover, L., III, 1971, Geology of the Coamo area, Puerto Rico, and its relation to the volcanic arc-trench association: U.S. Geological Survey Professional Paper 636, 102 p.

Grilli, S.T., M. Mohammadpour, L. Schambach, and A.R. Grilli, 2022, Tsunami coastal hazard along the U.S. East Coast from coseismic sources in Acores convergence zone and the Caribbean arc areas, Natural Hazards, v. 111, p. 1431-1478, https://doi.org/10.1007/s11069-021-05103-y

Grindlay, N. R., P. Mann, and J. Dolan, 1997, Researchers investigate submarine faults north of Puerto Rico, Eos, Trans. AGU, v. 78, p. 404.

Grindlay, N. R., M. Hearne, and P. Mann, 2005a, High risk of tsunami in the northern Caribbean, EOS, Transactions, American Geophysical Union, v. 26, n. 12, p. 121 and 126.

Grindlay, N. R., P. Mann, J. F. Dolan, and, J-P. van Gestel, 2005b, Neotectonic and subsidence of the northern Puerto Rico-Virgin Islands margin in response to the oblique subduction of high-standing ridges, *in* Mann, P., ed., Active tectonics and seismic hazards of Puerto Rico, the Virgin Islands, and offshore areas, Geol. Soc. Am. Special Paper 385, p. 31-60.

Grindlay, N. R., L. J. Abrams, L. Del Greco, and P. Mann, 2005c, Towards an integrated understanding of Holocene fault activity in western Puerto Rico: Constraints from high-resolution seismic and sidescan sonar data, *in* Mann, P., ed., Active tectonics and seismic hazards of Puerto Rico, the Virgin Islands, and offshore areas, Geol. Soc. Am. Special Paper 385, p. 139-160.

Hernández, D., 1985, Temblores y terromotos de Puerto Rico, Ponce, PR.

Jansma, P. E., G. S. Mattioli, A, Lopez, C. DeMets, T. H. Dixon, P. Mann, and E. Calais, 2000, Noetectonics of Puerto Rico and the Virgin Islands, northeastern Caribbean, from GPS geodesy, Tectonics, v. 6, p. 1021-1037.

Lander, J. F., L. S. Whiteside, and P. A. Lockridge, 2002, A brief tsunami history of tsunamis in the Caribbean Sea, The International Journal of the Tsunami Society, v. 20, n. 2, 57 p.

LaForge, R. C. and W. R. McCann, 2005, A seismic source model for Puerto Rico, for use in probabilistic ground motion hazard analyses, *in* Mann, P., ed., Active tectonics and seismic hazards of Puerto Rico, the Virgin Islands, and offshore areas: Geological Society of America Special Paper 385, p. 223-248.

Lynch, J. J., and R.R. Bodle, 1948, The Dominican earthquake of August, 1946, Bulletin of the Seismological Society of America, v. 38**,** p. 1-17.

Mann, P., C. Prentice, J.-C. Hippolyte, N. Grindlay, L. Abrams, and D. Lao-Davila, 2005, Reconnaissance study of Late Quaternary faulting along Cerro Goden fault zone, western Puerto Rico, in Mann, P., editor, Active tectonics and seismic hazards of Puerto Rico, the

Virgin Islands and Offshore areas, Geological Society of America Special Paper 385, p. 115-138.
McCann, W. R., 1985, On the earthquake hazards of Puerto Rico and the Virgin Islands, Seismological Society of America Bulletin, v. 75, p. 251-262.
McCann, W.R., 2003, Catolog of felt earthquakes for Puerto Rico and neighboring islands 1492-1899 with additional information for some 20th century earthquakes, Seismological Research Letter, v. 74, p. 199.
McIntyre, D. H., 1971, Geologic map of the Central La Plata Quadrangle, Puerto Rico, U.S. Geological Survey Miscellaneous Geolologic Investigations Series Map I-660, scale 1:20,000.
Mercado, A. N. R. Grindlay, P. Lynett, and P.L.-F. Liu, 2002, Investigation of the potential tsunami hazard on the north coast of Puerto Rico due to submarine landslides along the Puerto Rico Trench, Puerto Rico State Emergency Management Agency, Report, 432 p.
Miranda, E., J. Archbold, P. Heresi, A. Messina, I. Rosa, I. Robertson, K. Mosalam, T. Kijewski-Correa, D. Prevatt, and D. Roueche, 2020, StEER—Puerto Rico earthquake sequence December 2019 to January 2020: Field assessment structural team (FAST) early access reconnaissance report (EARR), *DesignSafe-CI*. doi: 10.17603/ds2-h0kd-5677.
Monroe, W. H., 1980, Geology of the middle Tertiary formations of Puerto Rico, USGS Professional Paper 953, 93 p.
Moya, J. C., 1998, The neotectonics of Western Puerto Rico, Ph.D. Dissertation, University of Colorado at Boulder, 132 p.
Moya, J. C., 1999, Results from neotectonic studies in western Puerto Rico, GSA Penrose Conference, Subduction to strike-slip transitions along plate boundaries, Dominican Republic, abstract volume http://www.uncwil.edu/people/grindlayn/penrose.html.
Moya, J. C., and W.R. McCann, 1991, Earthquake vulnerability study of Mayaguez, western Puerto Rico, Cooperative Agreement, Earthquake Safety Commission of Puerto Rico - Federal Emergency Management Agency, Internal Report 91-1: FEMAPR-0012. 66 p.
Mueller, C. S., A. D. Frankel, M. D. Petersen, and E. V. Leyendecker, 2003, Documentation for 2003 USGS seismic hazard maps of Puerto Rico and the U.S. Virgin Islands, USGS, Golden, Colorado, http://eqhazmaps.usgs.gov/html/prvi2003.html.
Mueller, C., A. Frankel, M. Petersen, and E. Leyendecker, 2010, New seismic hazard maps of Puerto Rico and the U.S. Virgin Islands, Earthquake Spectra, v. 26, n. 1, p. 169-185.
O'Loughlin, K. F., and J. F. Lander, 2003, Caribbean tsunamis-A 500-year history from 1498-1998, Kluwer Academic Publishers, The Netherlands.
Pilarczyk, J. E., and E. G. Reinhardt, 2012, Homotrema rubrum (Lamarck) taphonomy as an overwash indicator in marine ponds on Anegada, British Virgin Islands. Natural Hazards, v. 63, n. 1, p. 85-100. doi:10.1007/s11069-010-9706-3
Prentice, C. S., P. Mann, and G. Burr, 2000, Prehistoric earthquakes associated with a Late Quaternary in the Lajas Valley, Southwestern Puerto Rico, EOS Trans., American Geophysical Union, Annual Fall Meeting, p. F1182.
Prentice, C. S., H. Santos, P. Mann, M. Tuttle, E. Asencio, N. Grindlay, and J. Joyce, 2003a, Field trip: Recent tectonics and paleosesimology in western Puerto Rico, Seismological Society of America Annual Meeting, 52 p.
Prentice, C. S., P. Mann, L.R. Pena, G. Burr, 2003b, Slip rate and earthquake recurrence along the central Septentrional fault, North American-Caribbean plate boundary, Dominican Republic, Journal of Geophysical Research, v. 108, n. B3, 2149.

Prentice, C. S., and P. Mann, 2005, Paleoseismic study of the South Lajas fault: First documentation of an onshore Holocene fault in Puerto Rico, *in* Mann, P., ed., Active tectonics and seismic hazards of Puerto Rico, the Virgin Islands, and offshore areas, Geol. Soc. Am. Special Paper 385, p. 215-222.

Reid, H and S. Taber, 1919, The Puerto Rico earthquakes of October-November 1918, Bull. Seism. Soc. Amer., v. 9, p. 95-127.

Reimer, P. J., W. E. N. Austin, E. Bard, A. Bayliss, et al., 2020, The IntCal20 northern hemisphere radiocarbon age calibration curve (0-55 cal kBP), Radiocarbon, v. 62, n. 4, p. 725-757. doi: 10.1017/RDC.2020.41

Roig-Silva, C. M., E. Asencio, J. Joyce, 2013, The northwest trending north Boquerón Bay-Punta Montalva fault zone; A through going active fault system in southwestern Puerto Rico, Seismological Research Letters, v. 84, n. 3, p. 538-550.

Seed, H. B. and I. M. Idriss, 1971, Simplified procedure for evaluating soil liquefaction potential. Journal of the Soil Mechanics & Foundations Division (ASCE), v. 97 (SM9), p. 1249-1273.

Seyhan, E., 2015, NGA-West2 GMPEs validation tool, PEER, Berkley, CA.

ten Brink, U., W. Danforth, C. Polloni, and B. Andrews, 2004, New seafloor map of the Puerto Rico trench helps assess earthquake and tsunami hazards, EOS, Transactions, American Geophysical Union, v. 85, n. 37, p. 349-360.

ten Brink, U. S., W. H. Bakun, and C. H. Flores, 2011, Historical perspective on seismic hazard to Hispaniola and the northeast Caribbean region, J. Geophys. Res., v. 116, B12318, doi:10.1029/2011JB008497.

ten Brink, U. S., J. D. Chaytor, E. L. Geist, D. S. Brothers, and B. D. Andrews, 2014, Assessment of tsunami hazard to the U.S. Atlantic margin, Marine Geology, v. 353, p 31-54.

Tuttle, M. P., 2011, Study of source, magnitude, and recurrence time of large earthquakes affecting northern Puerto Rico: Collaborative research (MTA and USGS), Final Technical Report to US Geological Survey, EHP Award No. 06HQGR0023, 39 p.

Tuttle, M. P., Prentice, C. S., Dyer-Williams, K., Pena, L. R., and Burr, G., 2003, Late Holocene liquefaction features in the Dominican Republic: A powerful tool for earthquake hazard assessment in the northeastern Caribbean, Bulletin of the Seismological Society of America, v. 93, n. 1, p. 27-46.

Tuttle, M. P., Dyer-Williams, K., Schweig, E. S., Prentice, C. S., Moya, J. C., and Tucker, K. B., 2005a, Liquefaction induced by historic and prehistoric earthquakes in western Puerto Rico, *in* Mann, P., ed., Active tectonics and seismic hazards of Puerto Rico, the Virgin Islands, and offshore areas: Geological Society of America Special Paper 385, p. 263-276.

Tuttle, M. P., Dyer-Williams, K., Schweig, E.S., Moya, J.C., and Sims, J. D., 2005b, Paleoseismology of Puerto Rico from earthquake-induced liquefaction features: Collaborative research (MTA and USGS), Final Technical Report to US Geological Survey, EHP Award No. 00HQGR0004, 22 p.

Tuttle, M. and K. Dyer-Williams, 2006, Geological evaluation studies for the Rio Valenciano dam: Liquefaction study – phase one, Technical report prepared for CSA Group, 19 pages & appendices.

Tuttle, M. and K. Dyer-Williams, 2008, Geological evaluation studies for the Rio Valenciano dam: Liquefaction study – phase two, Technical report prepared for CSA Group, 29 pages & appendix.

Tuttle, M. P., Hartleb, R., Wolf, L., and P. W. Mayne, 2019, Paleoliquefaction studies and the evaluation of seismic hazard, Geosciences, v. 9, n. 7, 61 p, doi:10.3390/geosciences9070311.

Tuttle, M. and Z. Fuentes, 2021, Learning from Hurricane Irma, differentiating tsunami from hurricane deposits, and re-evaluating possible tsunami deposits on St. Thomas, US Virgin Islands, Final Technical Report to US Geological Survey, EHP Award No. G19AP00101, 58 p.

U.S. Geological Survey, Earthquake Hazards Program, 2017, Advanced National Seismic System (ANSS) comprehensive catalog of earthquake events and products: various, https://doi.org/10.5066/F7MS3QZH.

van Gestel, J-P, P. Mann, J. Dolan and N. R. Grindlay, 1998, Structure and tectonics of the upper Cenozoic Puerto Rico-Virgin Islands carbonate platform as determined from seismic reflection studies, J. Geophys. Res., v. 103, p. 30,505-30,530.

Wei, Y., 2022, Evaluating outer-rise earthquake hazards from the Puerto Rico Trench by calibrating inundation models with geologic evidence, Final Technical Report, Earthquake Hazard Reduction Program Award No. G20AP00049, p. 53, plus supplement.

Wei, Y., B. F. Atwater, U. ten Brink, and V. Roeber, 2016, Exploring the cause of catastrophic Caribbean inundation in 1200-1480 C.E. using numerical models compared with geological evidence, Abstract NH51D-03, 2016 Fall Meeting, AGU, San Francisco, California, 11-15 December.

Wells, D. L., and K. J. Coppersmith, 1994, New empirical relationships among magnitude, rupture length, rupture width, rupture area, and surface displacement, Bulletin of the Seismological Society of America, v. 84, p. 974–1002.

Williams, P.L., and M. Tuttle, 2010, Seismic hazard evaluation of the Northern Puerto Rico fault zone: A case study, Seismological Society of America, Eastern Section Meeting, Program and Abstracts, p. 48.

Youd, T. L., and I. M. Idriss, 2003, Liquefaction resistance of soils: Summary report from the 1996 NCEER and 1998 NCEER/NSF workshops on evaluation of liquefaction resistance of soils: Closure and Errata, Journal of Geotechnical and Geoenvironmental Engineering, v. 129, n. 3, 285 p.

Supplement

Evaluation of Scenario Earthquakes Using Liquefaction Potential Analysis

Scenario earthquakes of various moment magnitudes and distances are evaluated using the cyclic stress method for assessing liquefaction potential (e.g., Seed and Idriss, 1971 and 1982; Juang and Jiang, 2000; Youd et al., 2001; Youd and Idriss, 2003). This method has been the standard for evaluating liquefaction resistance of soils for more than thirty years and has been used in numerous paleoliquefaction studies (e.g., Green et al., 2005; Olson et al., 2005; Tuttle et al., 2005, 2019, and 2021). Given the interplate setting of Puerto Rico, ground motion prediction equations (GMPEs) and validation tool developed by the NGA-West2 project (e.g., Seyhan, 2015) are used to calculate peak ground accelerations for the scenario earthquakes.

After determining accelerations, cyclic stress ratios (CSR) generated by scenario earthquakes are calculated using Equation 1,

$$CSR_{7.5} = \frac{\tau_{ave}}{\sigma'_{vo}} = 0.65 \cdot \left(\frac{a_{max}}{g}\right) \cdot \left(\frac{\sigma_{vo}}{\sigma'_{v0}}\right) \cdot r_d \cdot \frac{1}{MSF} \quad (1)$$

where a_{max}=PGA (horizontal component), (a_{max}/g) is PGA divided by the acceleration due to gravity; σ_{vo} and σ'_{v0} are the total and effective vertical overburden stresses, respectively; r_d is a stress reduction coefficient; and MSF is the magnitude scaling factor. The $CSR_{7.5}$ represents the normalized shear stress $(\tau_{ave}/\sigma'_{vo})$ induced in the soil by the earthquake event (i.e., the seismic demand) and commonly referenced to a benchmark case with moment magnitude, **M** = 7.5.

In Puerto Rico, most of the soil or sediment selected for liquefaction potential analysis fall under site class D, or stiff soils, according to the National Earthquake Hazard Reduction Program (NEHRP) site classification (BSSC, 1997; Dobry et al., 2000). Furthermore, NEHRP recommends site class D be used where soil properties are not known in sufficient detail to make a site class determination. Therefore, site class D is applied to account for soil amplification effects at all sites. PGA (rock) was multiplied by the amplification factor, in this case 1.6, to obtain the a_{max} to be used in Equation 1. To further assess the possible role of soil amplification, site-specific response analysis would be required.

Variations in standard penetration test (SPT) procedure are corrected by adjusting the measured blow count (N_m) using Equation 2:

$$\boldsymbol{N_{1(60)} = C_N\, C_E\, C_B\, C_R\, C_S\, N_m} \quad (2)$$

where $N_{1(60)}$ is normalized blow count corrected for hammer energy (C_E), effective confining stress (C_N), borehole diameter (C_B), rod length (C_R), and sampler configuration (C_S), with N_m being the measured SPT resistance or "blow count" reported in blows/foot (or blows/0.3 m). In this way, the measured N value is standardized to 60% of the potential energy. The correction factors and blow counts are taken from the borehole logs.

Following the computations of the cyclic stress ratio and the adjustments and normalization of blow counts, the liquefaction potential of selected layers at borehole sites is determined by plotting CSR versus normalized blow count $[(N_1)_{60}]$ for **M** 7.5 earthquakes (Seed and Idriss, 1971). If CSR is greater than or equal to cyclic resistance ratio (CRR), the value plots on or above the curve, and the soil is likely to liquefy. Conversely, if CSR is less than CRR, the value plots below the curve, and liquefaction is considered unlikely.

In this study, the approximation to the base curve, the cyclic resistance ratio (CRR), is used. For clean sands, which are tested in boreholes using the SPT, CRR for an **M** 7.5 event proposed by Youd et al. (2001) is given by Equation 3:

$$CRR_{7.5} = \frac{1}{34 - (N_1)_{60-cs}} + \frac{(N_1)_{60-cs}}{135} + \frac{50}{\left[10\,.\,(N_1)_{60-cs} + 45\right]^2} - \frac{1}{200} \qquad (3)$$

for $(N_1)_{60\text{-}cs} < 30$; $(N_1)_{60\text{-}cs}$ refers to equivalent clean sand.

The CRR for magnitudes other than 7.5 is calculated by multiplying $CSR_{7.5}$ by the appropriate magnitude scaling factor (MSF), which is given by Equation 4, where M_w represents moment magnitude:

$$MSF = (M_w/7.5)^{-3.3} \qquad (4)$$

The following equation is used to calculate the value of the CRR for the evaluation of scenario earthquakes with magnitudes other than 7.5:

$$CRR = CRR_{M7.5} * MSF \qquad (5)$$

Once the CSR and the CRR are calculated, the factor of safety against liquefaction (FS_L) is determined using the following equation:

$$FS_L = \frac{CRR}{CSR} \qquad (6)$$

The calculated factor of safety (FS) is then used to approximately assess the probability of liquefaction (P_L). As proposed by Juang and Jiang (2000), the probability of liquefaction is calculated using Equation 7:

$$P_L = \frac{1}{1 + (FS\ /\ 1.0)^{3.34}}, \qquad (7)$$

where P_L is the probability of liquefaction and *Fs* is the factor of safety. If P_L is greater than or equal to 50%, a layer is likely to liquefy.

Tables

Table S1. Liquefaction sites along rivers in western and northwestern Puerto Rico.

Site*	Latitude °N Longitude °W	Cutbank Exposure	Liquefaction Features†	Weathering of Features	Constraining Dates ! & Events
Río Grande de Añasco					
RGA6	18.27054 67.11638	5 m high – well exposed, upper 3.5 m recent silt with plastic; lower 1.5 m interbedded silt and pebbley sand	One sand dike – 5 cm wide may terminate in sand sill or sand blow	Iron stained	Poorly constrained; given dating of sediment downstream, probably <A.D. 1422
RGA7	18.26634 67.12929	1 m high – upper 0.5 m vegetated, lower 0.5 m well exposed; silt	Three sand dikes – 3 cm, 1 cm, & 1 cm wide – larger dike pinches 0.3 m AWL or 0.7 m BTC	Iron stained	RGA10-C1: <A.D. 1644, high probability < A.D. 1720; probably A.D. 1918
RGA8	18.26846 67.13502	5 m high – very well exposed; silt	Two sand dike – 3 cm and 0.4 cm wide – daylights 2.5 m and 0.4 m AWL or 2.5 m and 4.6 m BTC	Not noted	RGA11-C3: <A.D. 1670, possibly <A.D. 1797: probably A.D. 1918
RGA9	18.27029 67.14604	3.2 m high – very similar to RGA10	One sand dike – 3 cm wide – pinches 1.3 m AWL or 1.9 m BTC	Iron stained	RGA11-C3: <A.D. 1670, possibly <A.D. 1797; probably A.D. 1918
RGA10	18.27099 67.14621	3.2 m high – very well exposed; silt with lenses of sand; buried soils	Three sand dikes – 13 cm, 4 cm, and 1 cm wide; pinch 0.8 m, 0.9 m, & 0.4 m AWL	Iron stained, some manganese	RGA10-C1: <A.D. 1644, high probability < A.D. 1720; probably A.D. 1918
RGA11	18.27219 67.14867	4 m high – upper 2 m vegetated, lower 2 m well exposed; inter-bedded clayey silt & fine sand	Two episodes of liquefaction; one sand blow – 12 cm thick – deposited 0.63 m AWL or 3.37 m BTC; two sand dikes – 5 cm & 3 cm wide – connected to sand blow; third dike – 4 cm wide – cross-	Iron stained	Younger sand dike – RGA11-C3: <A.D. 1670, probably <A.D. 1797; Sand blow – RGA11-C5: <A.D. 1644 Two events since

			cuts sand blow, becomes discontin-uous, & terminates 1.13 m AWL		A.D. 1644; probably A.D. 1670 & A.D. 1918
RGA12	18.27218 67.14877	3 m high – very well exposed; silt with thin interbeds of sand	One sand dike – 4 cm wide – extends at least 1.1 m AWL or 2 m BTC	Iron stained	RGA11-C3: <A.D. 1670, possibly <A.D. 1797; probably A.D. 1918
RGA13	18.27213 67.14897	3.7 m high – well exposed; interbedded silty clay & fine sand	Two sand dikes – 2 cm and 1 cm wide – larger dike daylights 1.47 m AWL or 2.23 m BTC; smaller dike also daylights	Not noted	RGA4-C1: <A.D. 1674, possibly <A.D. 1798; probably A.D. 1918
RGA20	18.27196 67.14886	2.3 m high – well exposed; silt and clayey silt with several lenses of fine sand	One sand dike – 20 cm wide at base & 9 cm wide near top; truncated at 1.46 m AWL or 0.84 m BTC	Iron stained	RGA11-C3: <A.D. 1670, possibly <A.D. 1797; probably A.D. 1918
RGA14	18.27202 67.14917	3 m high – upper 1.5 m vegetated, lower 1.5 m well exposed; silt	One sand dike – 4 cm wide – extends at least 1.1 m AWL or 1.9 m BTC	Iron stained; loose at base	RGA11-C3: <A.D. 1670, possibly <A.D. 1797; probably A.D. 1918
RGA15	18.27105 67.15104	3.8 m high –well exposed; inter-bedded silt & clayey silt with few interbeds of pebbley sand	One dike – 6 cm wide; dike extends at least 1.5 m AWL or 2.3 m BTC	Not noted	RGA4-C1: <A.D. 1674, possibly <A.D. 1798; probably A.D. 1918
RGA16	18.2693 67.15017	4.5 m high – lower 2 m very well exposed; interbedded silt & clay with few interbeds of sand	One sand blow – 6 cm thick – deposited 0.8 m AWL or 3.7 m BTC; one sand dike – 1 cm wide	Very iron stained	Similar to sand blow at RGA11; RGA11-C5: <A.D. 1644; probably A.D. 1670
RGA17	18.2696 67.15003	3.8 m high –well exposed; interbed-ded silt, clayey silt, & sand	One sand dike – 15 cm wide; dike pinches out at 1.8 m AWL or 2 m BTC	Iron stained	RGA4-C1: <A.D. 1674, possibly <A.D. 1798; probably A.D. 1918
RGA18	18.27058 67.15016	3 m high – upper 1 m vegetated, lower 2 m well	One sand dike – 16 cm wide; dike pinch out at 1.45 m AWL	Iron stained; loose throughout	RGA18-C1: high probability <A.D. 1636;

		exposed; interbedded silt and sand; buried soils	or 1.55 m BTC		RGA2-C2: <A.D. 1679, possibly <A.D. 1799; probably A.D. 1918
RGA19	18.27004 67.14871	3.5 m high – fairly well exposed; interbedded silt and sand; buried soils	One sand dike – 4 cm wide; pinches at 0.9 m AWL or 2.6 m BTC	Very iron stained; some fines coating of sand grains	RGA11-C5: <A.D. 1644; given weathering probably A.D. 1670
RGA4	18.26865 67.15142	3.4 m high – very well exposed; interbedded silt and sand; buried soils	Two sand dikes – 8 cm & 4.5 cm wide; dikes pinch out at 1.77 m and 1.6 m AWL or 1.63 m & 1.8 m BTC	Iron stained	RGA4-C1: <A.D. 1674, possibly <A.D. 1798; probably A.D. 1918
RGA3	18.26879 67.15167	3.2 m high – very well exposed; interbedded silt and sand; buried soils	One sand blow – 0.5 cm thick, partially eroded – deposited 1.64 m AWL or 1.56 m BTC; two sand dikes – 3 cm & 2.5 cm wide; possible source sand 40 cm BWL	Iron stained	RGA4-C1: <A.D. 1674 possibly, <A.D. 1798: probably A.D. 1918
RGA2	18.26971 67.15269	3.3 m high – very well exposed; silt with interbeds of sand & buried soils	One sand blow – 8 cm thick, partially eroded – deposited about 1 m AWL or 2.3 m BTC; two sand dikes – 13 cm & 1 cm wide	Iron stained	similar to sand blow at RGA16; RGA2-C2: >A.D. 1679-1941; probably A.D. 1670
RGA1	18.27194 67.15304	4.6 m high – very well exposed; silt with interbeds of sand & buried soils	One sand dike – 3.5 cm wide becomes discontinuous and terminated 1.6 m AWL or 3 m BTC; possible source sand 80 cm BWL	Iron stained	RGA4-C1: <A.D. 1674, possibly <A.D. 1798: probably A.D. 1918
Río Culebrinas					
RC2	18.3757 67.1174	5.1 m high – very well exposed; interbedded silt & sand with 4-6 buried soils	One sand blow – 1 cm thick – probably partially eroded; two sand dikes – 6, 2 cm wide; largest dike crosscuts buried soil & broadens into base	Not noted	RC2-C1; <A.D. 1640, high probability <A.D. 1722; probably A.D. 1918

			of sand blow 3 m AWL or 2.1 m BTC		
RC3	18.37674 67.1193	4.8-5.3 m high – very well exposed; silt with seven buried soils	Two sand dikes – 4 and 1.5 cm wide; dikes terminate 1.39 m AWL (~3.36 m BTC) in 5th buried soil	Iron staining on sand grains in dike; loose	RC3-C2: <A.D. 1296; poorly constrained <A.D. 1296
RC100	18.37604 67.11758	5 m high – lower 2 m well exposed & upper 3 m vegetated; silt with several interbeds of sand & at least two buried soils	One sand dike – 8 cm wide; pinches out 1.6 m AWL or 3.4 m BTC	Iron stained	Similar to RC3; RC3-C2: <A.D. 1296; poorly constrained <A.D. 1296
RC4	18.37926 67.12212	4.7 m high – very well exposed; silt with six buried soils	One sand dike – 4.5 cm wide; pinches out 1.4 m AWL or 3.3 m BTC	Iron stained	Similar to RC3; RC3-C2: <A.D. 1296; poorly constrained <A.D. 1296
RC5	18.37877 67.12344	4.8 m high – very well exposed; silt with six buried soils	One sand dike – 8 cm wide; pinches out 2.3 m AWL or 2.5 m BTC	Not noted	RC6-C3: <A.D. 1401: likely either A.D. 1670 or AD 1918
RC101	18.38203 67.12594	8 m high – very well exposed; silt with 7 paleosols	One sand dike – 12 cm wide; dike extends to 1 m AWL or 7 m BTC, appears to daylight	Iron stained throughout dike	RC101-C1: <A.D. 1053, high probability <A.D. 1156; poorly constrained < A.D. 1156
RC6	18.38442 67.12869	4.4 m high – very well exposed; clayey silt with paleosols	Five sand dikes – ranging from 1.5 to 3 cm wide; one dike extends to 2.6 m AWL or 1.8 m BTC	Iron stained; loose	RC6-C3: <A.D. 1401; likely either A.D. 1670 or AD 1918
RC102	18.38832 67.13261	5.3 m high – very well exposed; interbedded silt & sandy silt; at least 4 buried soils	One sand dike – 3 cm wide; terminates at 2.5 m AWL or 2.8 m BTC	Iron stained; loose at base, not loose in tip	RC6-C3: <A.D. 1401; likely either A.D. 1670 or AD 1918
RC7	18.38832 67.13268	Not noted but similar to nearby RC102 & RC8–	Nine sand dikes – largest dike 3 cm wide; dikes extend to	Not noted	<A.D. 1053, high probability <A.D. 1156; poorly

		upper part of largest dike covered by slump	~1 m AWL then covered by slump		constrained < A.D. 1156
RC8	18.38942 67.13314	4.7 m high – very well exposed; interbedded clayey silt & sandy silt; buried soils	One sand dike – 5 cm wide; terminates 1.8 m AWL, 2.9 m BTC	Not iron stained; loose	RC3-C2: <A.D. 1296; poorly constrained <A.D. 1296
RC9	18.38579 67.13582	Similar to nearby site RC8	One sand dike – 1.5 cm wide; extends only 0.2 m AWL, tip may be covered by slump	Not iron stained; loose	Similar to RC8; likely formed < A.D. 1296
RC10	18.38579 67.13706	Similar to nearby sites RC9 & RC8; silty clay with buried soils	Five sand dikes – ranging from 0.5 to 3 cm wide; all dike tips either daylight or covered by slump	Loose	Similar to RC8 & RC9; likely formed < A.D. 1296
RC103	18.39019 67.14146	4.97 m high – well exposed; interbedded silt & sand; buried soil 3.47 m AWL	One sand dike – 2 cm wide; terminates at 2.2 m AWL or 2.8 m BTC	Iron stained; loose	RC6-C3: <A.D. 1401; likely either A.D. 1670 or AD 1918
RC1	18.399 67.15681	3.1 m high – very well exposed; interbedded silt & sand; buried soil	One sand blow – 20 cm thick – deposited on buried soil 1.6 m AWL or 1.5 m BTC; six sand dikes – 23, 10, 7, 3, 3, 2 cm wide; largest dike extends through buried soil & forms vent structure at base of sand blow	Iron stained & accumulation of fines on sand grains in sand blow and sand dikes	RC1-C3: <A.D. 1304, no known large events in PR region during Spanish colonization from A.D. 1508 until A.D. 1670 event; A.D. 1304-1508
RC11	18.39923 67.15766	3.9 m high – very well exposed; silt, with interbeds of sand, several buried soils	Seven sand dikes – 18 12, 6, 4, 4, 3, 2.5 cm wide; largest dike terminates 1.75 m AWL or 2.15 m BTC	Iron stained & accumulation of fines	RC11-C3: <A.D. 1516, probably A.D. 1670
RC12	18.39938 67.15775	3.7 m high – very well exposed; silt, with interbeds of sand, several buried soils	Three sand dikes – 7, 4, 2.5 cm wide; dikes terminate 1.3, 1.2, 0.2 m AWL or 2.4, 2.5, and 3.5 m BTC, respectively	Iron stained & accumulation of fines	Similar to RC1; RC1-C3: <A.D. 1304, probably A.D. 1304-1508

RC13	18.40017 67.16224	2.7 m high –well exposed; silt, with interbeds of sand, several paleosols	One sand blow – 12 cm thick deposited on buried soil 1.2 m AWL or 1.5 m BTC; two sand dikes – 8, 1 cm wide; source sand of dikes at 20-30 m AWL	Iron stained	RC13-C3: <A.D. 1679, likely <A.D. 1752; probably A.D. 1918
Río Guanajibo					
RG1	18.13374 67.14064	3.3 m high –well exposed; silt with interbeds of sand with buried soils	One sand dike – 3 cm pinches at 1 m AWL or 2.3 m BTC	Iron stained and mottled	Given dating of similar sediment along Río Grande de Añasco, probably <A.D. 1422
RG2	18.15477 67.16435	2.5 m high – well exposed; clayey silt with buried soils	One sand dike – 0.5 cm daylights	Not noted	Given dating of similar sediment along Río Grande de Añasco, probably <A.D. 1422
Río Grande de Manatí					
RGM1	18.44213 66.52921	6 m high – very well exposed; silt and clayey silt with six buried soils	One sand blow – 22 cm thick – deposited 2 m AWL or 4 m BTC; feeder dike of sand blow – 10-34 cm wide; 0.5 cm wide dike daylights at 1.5 m AWL or 4.5 BTC	All features weathered throughout: iron and manganese stained; fines accumulation	RM1-S2: >410 B.C; RM1-S1: <1201 B.C., possibly <1133 B.C.: probably 1201-410 B.C.
RGM2N	18.44187 66.53231	5.64 m high – very well exposed; silt with six buried soils	Three generations of sand dikes; four sand dikes – 40 cm, 3 cm, 2.5 cm, & 1.5 cm wide; graben above largest dike disturbs buried soil at 2.24 m AWL; base of overlying buried soil also disturbed but not top of soil at 2.64 m AWL; youngest dikes pinches out ~2 m AWL	Largest & oldest sand dike – very iron stained & mottled; 2nd generation dikes – iron stained & mottled; youngest dikes – relatively un-weathered	Large sand dike & related graben - RGN2N-S1: >A.D. 546; RGM2N-S2: <1436 B.C.; probably same event at RGM1 1201-410 BC; Two younger generations sand dikes - probably A.D. 1304-1508 & A.D. 1787

RGM2S	18.44004 66.53176	6 m high – well-exposed; silt with three buried soils overlying silty sand	One sand dike – 1 cm wide – pinches out at 1.2 m AWL or 4.8 m BTC	Slightly iron stained; loose	Similar to youngest generation dikes at RGM2N; probably A.D. 1787
RGM5N	18.44825 66.53336	3.4 m high – vegetated; upper 2 m disturbed; lower 1.4 m interbedded clayey silt, silt, and sandy silt	One sand dike – 14-31 cm wide – forms sills at 1.2 m AWL or 2.2 m BTC; sill – 3 cm thick and 20 cm long	Slightly iron stained; loose	RGM4N-C2: <A.D. 1038; probably A.D. 1787
RGM5S	18.44753 66.53462	2.8 m high – vegetated; upper 1.2 m disturbed; lower 1.6 m silt with few layers of silty sand	One sand dike – 4 cm wide may form sill at 1.6 m AWL or 1.2 m BTC	Upper 15 cm of dike iron stained; some accumulation of fines; loose below	RGM4N-C2: <A.D. 1038; probably A.D. 1787
RGM4N	18.46116 66.53184	2.1 m high – well-exposed; silt with three buried soils	Two sand dikes – 4 cm and 1.2 cm wide – pinch at 1.4 m and 0.6 m AWL or 0.7 m and 1.5 m BTC	Mottled throughout dikes	Similar to middle generation dike at RGM2N; RGM4N-C2: <A.D. 1038; probably A.D. 1304-1508
Río de la Plata					
RLP10	18.43264 66.25755	4 m high – very well-exposed; several fining upward sequences of very fine sand to silt; buried soils	Three sand dikes – 1.5 cm, 0.5 cm, 0.5 cm wide; largest dike pinches at 2 m AWL or 2 m BTC	Upper 65 cm of largest dike very iron stained & mottled	Similar to middle generation dike at RGM2N; RLP10-C2: <A.D. 640; probably A.D. 1304-1508

* Sites organized according to position along river; first site is farthest upstream.

! Calendar dates: < means features formed since; > means features formed before; event assignments based on dating, position in cutbank, and weathering of liquefaction features; additional comments provided in the Puerto Rico liquefaction database available at http://mptuttle.com/databases.html.

† Abbreviations: AWL – above water level; BWL – below water level; BTC – below top of cutbank.

Table S2. Results of radiocarbon dating of samples collected at study sites along rivers.

Site Sample Lab Sample	$^{13}C/^{12}C$ Ratio	^{14}C Age Yr B.P.[1]	Cal Age Yr B.P.[2]	Cal Date A.D./B.C.[2]	Probability[2]	Sample Description[3]
Río Grande de Añasco						
RGA2-C2 BA-129693	-27.2	100 ± 40	271-209 198-186 151-9	AD 1679-1741 AD 1752-1764 AD 1799-1941	26.3 2.1 67	Charred material few cm above top of sand blow; 1.03 m AWL
RGA4-C1 BA-129691	-11.4	110 ± 40	276-206 200-185 176-174 152-8	AD 1674-1744 AD 1750-1765 AD 1774-1776 AD 1798-1942	26.8 3.1 0.4 65.1	Charred material 6 cm below dike tip, 1.54 m AWL
RGA4-C3 BA-129694	-17.8	420 ± 40	528-426 378-320	AD 1422-1524 AD 1572-1630	77.1 18.3	Charred material 23 cm below dike tip; 1.47 m AWL, 2.03 m BTC
RGA4-O4 BA-146693	-26.7	90 ± 40	270-210 198-187 150-10	AD 1680-1740 AD 1752-1763 AD 1800-1940	26.2 1.5 67.7	Possibly recent deposit; leaves 1.77 m below top of dike; just AWL
RGA10-C1 BA-146694	-28.5	190 ± 40	306-250 230-134 117-60 43-Post 0	AD 1644-1700 AD 1720-1816 AD 1833-1890 AD 1907-Post 1950	21.7 46.3 9.9 17.5	Charred material 50 cm below top of dike that extends highest in cutbank; 0.4 m AWL
RGA11-C3 BA-146695	-28.4	130 ± 40	280-171 153-6	AD 1670-1779 AD 1797-1944	36 59.4	Charred material 10 cm below tip of younger sand dikes and 28 cm above sand blow; 1.03 m AWL
RGA11-C5 BA-146696	-28.0	190 ± 40	306-250 230-134 117-60 43-Post 0	AD 1644-1700 AD 1720-1816 AD 1833-1890 AD 1907-Post 1950	21.7 46.3 9.9 17.5	Charred material 10 cm below sand blow; 0.53 m AWL
RGA18-C1 BA-146697	-31.4	200 ± 50	418-414 314-54 48-Post 0	AD 1532-1536 AD 1636-1896 AD 1902-Post 1950	0.4 79 16	Charred material 1.25 m below tip of sand dike; 0.2 m AWL
Río Culebrinas						
RC1-C3 BA-129692	-21.7	560 ± 40	646-585 567-516	AD 1304-1365 AD 1383-1434	50.2 45.2	Charred material from buried soil, 10 cm below sand blow, 1.5 m AWL, 1.6 m BTC
RC1-W1 BA-146689	-26.4	160 ± 80	422-410 316-Post 0	AD 1528-1540	0.9 94.5	Wood, possibly in recent deposit

				AD 1634-Post 1950		along base of bank, 1 m below top of dike, 3 m BTC
RC2-C1 BA-146690	-26.5	200 ± 40	310-251 228-136 116-64 42-Post 0	AD 1640-1699 AD 1722-1814 AD 1834-1886 AD 1908-Post 1950	24.6 47.2 7.1 16.5	Charred material 14 cm below sand blow, 2.86 m AWL, 2.24 m BTC
RC3-C2 BA-146691	-16.2	600 ± 40	654-536	AD 1296-1414	95.4	Charred material adjacent to top of sand dike; 1.39 m AWL, 3.36 m BTC
RC6-C3 BA-146692	-18.2	460 ± 40	549-450 350-334	AD 1401-1500 AD 1600-1616	93.4 2	Charred material 27 cm below termination of uppermost sand dike; 2.28 m AWL, 2.07 m BTC
RC11-C3 BA-177892	-26.7	240 ± 40	434-360 330-260 222-141 29-Post 0	AD 1516-1590 AD 1620-1690 AD 1728-1809 AD 1921-Post 1950	14.4 38.9 33.8 8.3	Charred material 3 cm below dike termination or 1.72 m AWL, 2.18 m BTC
RC13-C2 BA-177893	-25.3	190 ± 40	306-250 230-134 117-60 43-Post 0	AD 1644-1700 AD 1720-1816 AD 1833-1890 AD 1907-Post 1950	21.7 46.3 9.9 17.5	Charred material collected 22 cm above sand blow, 1.42 m AWL, 1.28 m BTC
RC13-C3 BA-177894	-26.8	100 ± 40	271-209 198-186 151-9	AD 1679-1741 AD 1752-1764 AD 1799-1941	26.3 2.1 67	Charred material from buried soil 12 cm below sand blow, 0.96 m AWL 1.74 m BTC
RC101-C1 BA-220013	-28.3	830 ± 40	897-889 794-672	AD 1053-1061 AD 1156-1278	1.1 94.3	Charred material 20 cm below dike termination, 0.8 m AWL, 7.2 m BTC
Río Grande de Manatí						
RGM1-S2 BA-178003	-17.5	2450 ± 40	2705-2628 2620-2555 2547-2359	756-679 BC 671-606 BC 598-410 BC	24.6 16.4 54.4	Organic sediment 0-3 cm above sand blow, 2.2 m AWL, 3.8 m BTC
RGM1-S1 BA-178002	-18.3	2880 ± 40	3150-3091 3082-2879	1201-1142 BC 1133-930 BC	11.6 83.3	Organic sediment 0-3 cm below sand blow, 2 m AWL, 4 m BTC
RGM2N-S1 BA-197703	-18.6	1670 ± 70	1707-1404	AD 243-546	95.4	Organic sediment 2.64 m AWL, 3 m BTC; uppermost

						centimeter of undisturbed buried soil above graben
RGM2N-S2 BA-197704	-15.8	3050 ± 60	3385-3073	1436-1124 BC	95.4	Organic sediment 2.24 m AWL, 3.4 m BTC; uppermost centimeter of buried soil disturbed by graben
RGM2N-C1 BA-197702	-25.4	4420 ± 40	5279-5168 5135-5102 5070-4865	3330-3219 BC 3186-3153 BC 3121-2916 BC	20.9 4.4 70.1	Charred material collected 0.49 m AWL, 5.15 m BTC from silt in top of large sand dike
RGM4N-C2 BA-197705	-26.8	910 ± 40	912-734	AD 1038-1216	95.4	Charred material collected 95 cm below tip of larger sand dike; 0.5 m AWL
Río de la Plata						
RLP10-C1 BA-197699[4]	-25.4	152.1 ± 0.6 pMC	Post 0	AD 1963.2-1963.3 AD1968.4-1968.5 AD1968.9-1969.0 AD 1969.3 AD 1969.6-1969.8 AD 1970-1971.1 AD 1971.3-1972.2	5.5 0.4 6.6 0.1 8.2 50.7 28.5	Charred material from root cast through sand dike
RLP10-C2 BA-197700	-25.5	1340 ± 40	1310-1176	AD 640-774	95.4	Charred material from silt 20 cm below sand dike tip, 1.8 m AWL, 2.2 m BTC
Río Espiritu Santo-Grande						
RGR1-W1 BA-197701	-25.3	1570 ± 60	1568-1342 1328-1312	AD 382-608 AD 622-638	94.1 1.3	Charred material from burned log in sandy silt 6.3 m BTC
Río Blanco						
RB1-C1 BA-242404	-27.8	70 ± 40	267-215 148-14	AD 1683-1735 AD 1802-1936	26.7 68.7	Wood collected from sandy silt about 2.7 m BTC
Río Gurabo						
RG8-C3 BA-242406	-26.8	1590 ± 40	1538-1384	AD 412-566	95.4	Plant material collected ~6 m BTC from peat layer

Río Valenciano						
RV3-C1 BA-243249	-15.1	2960 ± 40	3318-3306 3239-2994 2980-2967	1369-1357 BC 1290-1045 BC 1031-1018 BC	1.1 93.1 1.3	Charred material collected ~4.5 m BTC from clayey silt

[1] Conventional radiocarbon ages in years B.P. or before present (1950) determined by Beta Analytic, Inc. Errors represent 1 standard deviation statistics or 68% probability.

[2] Calibrated age ranges as determined by Beta Analytic, Inc., using the high probability density range method (Bronk Ramsey, 2009) and INTCAL20 (Reimer et al., 2020). Ranges represent 2 standard deviation statistics or 95.4% probability.

[3] Abbreviations: AWL – above water level; BTC – below top of cutbank

[4] Calibrated age ranges for Post-0 values from Hua et al. (2013) using IntCal13 from Reimer et al. (2013). Ranges represent 2 standard deviation statistics or 95.4% probability.

Table S3. Description of sediment at borehole location along surveyed rivers and used in liquefaction potential analysis.

River Location Borehole No.	Map ID[1]	Depth (m)	Description of Susceptible Sediment	Blow Count (N)[2]
Culebrinas PR 2 bridge BH S4	1	4.6 6.1	gray, loose, silty sand, coarse grained, and gravel, fine grained, sub-angular, trace clay brown and gray, medium silty sand, fine to coarse grained, gravelly, fine grained, sub-angular, trace clay	9 11
Anasco PR 406 bridge BH 9	2	3.1 4.6	brown, medium to coarse sand brown, fine sand, trace fine gravel	13 3
Anasco PR 430 bridge BH13	3	3.1 6.1 7.6 10.7 13.7 15.2	brown, medium sand brown, medium sand, trace gravel, some clay brown, medium sand, trace gravel, some clay grayish brown, fine sand, grayish brown, fine sand grayish brown, fine sand	4 20 12 6 10 5
Guanajibo PR 114 bridge BH RG 4	4	5.5 7.3	sand, fine grained, little clay lumps, dark brown sand, fine grained, no clay lumps, very dark gray	3 21
Grande de Manati PR 22 bridge BH 109	5	7.6 9.1 10.7	dark gray, coarse sand with some fine gravel dark gray, fine to medium, silty sand dark gray, fine to medium, silty sand	13 8 7
de la Plata PR 165 bridge BH VC 9	6	3.0 4.6	brown, loose to medium dense, silty sand, little fine gravel brown, loose to medium dense, silty sand, little fine gravel	9 17
de la Plata PR 22 bridge BH 16	7	1.5 3.0 4.6 6.1 7.6	medium to coarse sand and gravel, trace silt, loose, brown medium to coarse sand and gravel, trace silt, loose, brown medium to coarse, sand and gravel, medium, olive brown medium to coarse, sand and gravel, medium, olive brown medium to coarse, sand and gravel, medium, olive brown	9 10 13 15 13
Gurabo Connector PR 31 & PR 185 bridge BH 4	8	3.4 5.8	sand, little silt and sub rounded to rounded gravel, loose, brownish gray sand, some sub rounded to rounded gravel, trace silt, medium dense, brown	5 11

		7.3	sand, some sub rounded to rounded gravel, trace silt, medium dense, brown	14
Blanco PR 53 bridge BH 9	9	3.0	brown and gray, loose to medium sand, fine to coarse grained, some silt and clay, little gravel, fine grained,	10
		4.6	gray, loose sand, fine to coarse grained, gravelly, fine grained, little silt, trace clay	6
		6.1	gray, medium sand, fine to coarse grained, gravelly, fine grained, sub angular, some silt trace clay	14
		7.6	gray, medium sand, with olive and gray very stiff clay	24

[1] Borehole locations shown on Figure 5 and Figures S1-S5 in the Supplement.

[2] Blow count (N) is the total number of blows required to drive a split spoon sampler 0.3 m using standard hammer (63.5 kg) dropping 0.76 m.

Table S4. Results of liquefaction potential analysis of the 1918 earthquake with ANSS location (U.S. Geological Survey, 2017) as source (Figure 8).

Site Name	Map ID*	Distance† (km)	Results‡, § (WT@ 1 m) ‖, #	Results‡, § (WT@ 3 m) ‖
Scenario earthquake M 7.1				
Río Culebrinas	1	45.5	N	N
Río Grande de Añasco	2	58.7	L	N
Río Grande de Añasco	3	59.0	L/N	N
Río Guanajibo	4	73.9	N	N
Río Grande de Manatí	5	82.5	N	N
Río de la Plata	6	108.4	N	N
Río de la Plata	7	109.8	N	N
Scenario earthquake M 7.4				
Río Culebrinas	1	45.5	L	N
Río Grande de Añasco	2	58.7	L	L
Río Grande de Añasco	3	59.0	L	L/N
Río Guanajibo	4	73.9	L	N
Río Grande de Manatí	5	82.5	N	N
Río de la Plata	6	108.4	N	N
Río de la Plata	7	109.8	N	N

* Borehole locations shown on Figure 5 and Figures S1-S5 in the Supplement.

† Distance between scenario earthquake considered and geotechnical site data used in the analysis.

‡ L = Liquefaction likely for 45% - 100% of the layers analyzed; L/N = marginal because liquefaction predicted for 24% - 44% of the layers analyzed; N = liquefaction not likely because liquefaction predicted for less than 24% of the layers analyzed.

§ See electronic supplement for detailed description of liquefaction potential analysis and tables of results.

‖ WT = water table; depth used in liquefaction potential analysis.

Table S5. Results of liquefaction potential analysis of the 1787 earthquake with ten Brink et al. (2011) location 2 as source (Figure 8).

Site Name	Map ID*	Distance† (km)	Results‡, § (WT@ 1 m) ‖, #	Results‡, § (WT@ 3 m) ‖
Scenario earthquake M 6.4				
Río Culebrinas	1	108.5	N	N
Río Grande de Añasco	2	128.8	N	N
Río Grande de Añasco	3	130.4	N	N
Río Grande de Manatí	5	43.8	N	N
Río de la Plata	6	17.5	N	N
Río de la Plata	7	21.0	N	N
Río Gurabo	8	44.3	N	N
Río Blanco	9	55.3	N	N

* Borehole locations shown on Figure 5 and Figures S1-S5 in the Supplement.

† Distance between scenario earthquake considered and geotechnical site data used in the analysis.

‡ L = Liquefaction likely for 45% - 100% of the layers analyzed; L/N = marginal because liquefaction predicted for 24% - 44% of the layers analyzed; N = liquefaction not likely because liquefaction predicted for less than 24% of the layers analyzed.

§ See electronic supplement for detailed description of liquefaction potential analysis and tables of results.

‖ WT = water table; depth used in liquefaction potential analysis.

Table S6. Results of liquefaction potential analysis of 1787 earthquake with USGS location (Mueller et al., 2003) as source (Figure 8).

Site Name	Map ID*	Distance† (km)	Results‡, § (WT@ 1 m) ‖, #	Results‡, § (WT@ 3 m) ‖
Scenario earthquake M 7.7				
Río Culebrinas	1	138.7	N	N
Río Grande de Añasco	2	142.0	N	N
Río Grande de Añasco	3	143.7	N	N
Río Grande de Manatí	5	83.0	L	L
Río de la Plata	6	65.4	N	N
Río de la Plata	7	69.4	N	N
Río Gurabo	8	84.1	L/N	N
Río Blanco	9	89.8	N	N
Scenario earthquake M 8.0				
Río Culebrinas	1	138.7	N	N
Río Grande de Añasco	2	142.0	N	N
Río Grande de Añasco	3	143.7	N	N
Río Grande de Manatí	5	83.0	L	L
Río de la Plata	6	65.4	L	N
Río de la Plata	7	69.4	L/N	N
Río Gurabo	8	84.1	L	L/N
Río Blanco	9	89.8	L/N	L/N

* Borehole locations shown on Figure 5 and Figures S1-S5 in the Supplement.

† Distance between scenario earthquake considered and geotechnical site data used in the analysis.

‡ L = Liquefaction likely for 45% - 100% of the layers analyzed; L/N = marginal because liquefaction predicted for 24% - 44% of the layers analyzed; N = liquefaction not likely because liquefaction predicted for less than 24% of the layers analyzed.

§ See electronic supplement for detailed description of liquefaction potential analysis and tables of results.

‖ WT = water table; depth used in liquefaction potential analysis.

Table S7. Results of liquefaction potential analysis of 1670 earthquake with Cerro Godin fault north of Añasco as source (Figure 8).

Site Name	Map ID*	Distance† (km)	Results‡, § (WT@ 1 m) ‖, #	Results‡, § (WT@ 3 m) ‖
Scenario earthquake M 6.0				
Río Culebrinas	1	10.4	L/N	N
Río Grande de Añasco	2	4.3	L	L
Río Grande de Añasco	3	3.6	L	L
Río Guanajibo	4	17.9	L	L
Río Grande de Manatí	5	66.5	N	N
Scenario earthquake M 6.2				
Río Culebrinas	1	10.4	L	L
Río Grande de Añasco	2	4.3	L	L
Río Grande de Añasco	3	3.6	L	L
Río Guanajibo	4	17.9	L	L
Río Grande de Manatí	5	66.5	N	N

* Borehole locations shown on Figure 5 and Figures S1-S5 in the Supplement.

† Distance between scenario earthquake considered and geotechnical site data used in the analysis.

‡ L = Liquefaction likely for 45% - 100% of the layers analyzed; L/N = marginal because liquefaction predicted for 24% - 44% of the layers analyzed; N = liquefaction not likely because liquefaction predicted for less than 24% of the layers analyzed.

§ See electronic supplement for detailed description of liquefaction potential analysis and tables of results.

‖ WT = water table; depth used in liquefaction potential analysis.

Table S8. Results of liquefaction potential analysis of 1670 earthquake with fault east of Mayaguez as source (Figure 8).

Site Name	Map ID*	Distance† (km)	Results‡, § (WT@ 1 m) ‖, #	Results‡, § (WT@ 3 m) ‖
Scenario earthquake M 6.0				
Río Culebrinas	1	23.4	N	N
Río Grande de Añasco	2	13.9	L	L
Río Grande de Añasco	3	14.3	L	L/N
Río Guanajibo	4	11.5	L	L
Río Grande de Manatí	5	61.5	N	N
Scenario earthquake M 6.5				
Río Culebrinas	1	23.4	N	N
Río Grande de Añasco	2	13.9	L	L
Río Grande de Añasco	3	14.3	L	L
Río Guanajibo	4	11.5	L	L
Río Grande de Manatí	5	61.5	N	N

* Borehole locations shown on Figure 5 and Figures S1-S5 in the Supplement.

† Distance between scenario earthquake considered and geotechnical site data used in the analysis.

‡ L = Liquefaction likely for 45% - 100% of the layers analyzed; L/N = marginal because liquefaction predicted for 24% - 44% of the layers analyzed; N = liquefaction not likely because liquefaction predicted for less than 24% of the layers analyzed.

§ See electronic supplement for detailed description of liquefaction potential analysis and tables of results.

‖ WT = water table; depth used in liquefaction potential analysis.

Table S9. Results of liquefaction potential analysis of 1670 earthquake with South Lajas fault southwest of San Germán as source (Figure 8).

Site Name	Map ID*	Distance† (km)	Results‡, § (WT@ 1 m) ‖, #	Results‡, § (WT@ 3 m) ‖
Scenario earthquake M 6.7				
Río Culebrinas	1	42.7	N	N
Río Grande de Añasco	2	29.7	L	L
Río Grande de Añasco	3	28.9	L	L/N
Río Guanajibo	4	14.4	L	L
Río Grande de Manatí	5	79.7	N	N

* Borehole locations shown on Figure 5 and Figures S1-S5 in the Supplement.

† Distance between scenario earthquake considered and geotechnical site data used in the analysis.

‡ L = Liquefaction likely for 45% - 100% of the layers analyzed; L/N = marginal because liquefaction predicted for 24% - 44% of the layers analyzed; N = liquefaction not likely because liquefaction predicted for less than 24% of the layers analyzed.

§ See electronic supplement for detailed description of liquefaction potential analysis and tables of results.

‖ WT = water table; depth used in liquefaction potential analysis.

Table S10. Results of liquefaction potential analysis of A.D. 1304-1508 earthquake with North America plate interface northwest of Puerto Rico as source (A on Figure 8).

Site Name	Map ID*	Distance† (km)	Results‡, § (WT@ 1 m) ‖, #	Results‡, § (WT@ 3 m) ‖
Scenario earthquake M 8.0				
Río Culebrinas	1	82.7	L	N
Río Grande de Añasco	2	96.2	L	L
Río Grande de Añasco	3	96.1	L	L/N
Río Grande de Manatí	5	116.4	L	L/N
Río de la Plata	6	139.8	N	N
Río de la Plata	7	141.5	N	N
Río Gurabo	8	183.9	N	N
Río Blanco	9	197.6	N	N
Scenario earthquake M 8.5				
Río Culebrinas	1	82.7	L	L
Río Grande de Añasco	2	96.2	L	L
Río Grande de Añasco	3	96.1	L	L
Río Grande de Manatí	5	116.4	L	L
Río de la Plata	6	139.8	N	N
Río de la Plata	7	141.5	N	N
Río Gurabo	8	183.9	N	N
Río Blanco	9	197.6	N	N

* Borehole locations shown on Figure 5 and Figures S1-S5 in the Supplement.

† Distance between scenario earthquake considered and geotechnical site data used in the analysis.

‡ L = Liquefaction likely for 45% - 100% of the layers analyzed; L/N = marginal because liquefaction predicted for 24% - 44% of the layers analyzed; N = liquefaction not likely because liquefaction predicted for less than 24% of the layers analyzed.

§ See electronic supplement for detailed description of liquefaction potential analysis and tables of results.

‖ WT = water table; depth used in liquefaction potential analysis.

Table S11. Results of liquefaction potential analysis of A.D. 1304-1508 earthquake with eastern Septentrional fault northwest of Puerto Rico as source (B on Figure 8).

Site Name	Map ID*	Distance† (km)	Results‡, § (WT@ 1 m) ‖, #	Results‡, § (WT@ 3 m) ‖
Scenario earthquake M 8.0				
Río Culebrinas	1	119.1	N	N
Río Grande de Añasco	2	130.2	L	N
Río Grande de Añasco	3	129.0	L	L/N
Río Grande de Manatí	5	173.3	N	N
Río de la Plata	6	201.5	N	N
Río de la Plata	7	202.4	N	N
Río Gurabo	8	244.5	N	N
Río Blanco	9	258.5	N	N
Scenario earthquake M 8.5				
Río Culebrinas	1	119.1	L	L
Río Grande de Añasco	2	130.2	L	L
Río Grande de Añasco	3	129.0	L	L
Río Grande de Manatí	5	173.3	L	N
Río de la Plata	6	201.5	N	N
Río de la Plata	7	202.4	N	N
Río Gurabo	8	244.5	N	N
Río Blanco	9	258.5	N	N

* Borehole locations shown on Figure 5 and Figures S1-S5 in the Supplement.

† Distance between scenario earthquake considered and geotechnical site data used in the analysis.

‡ L = Liquefaction likely for 45% - 100% of the layers analyzed; L/N = marginal because liquefaction predicted for 24% - 44% of the layers analyzed; N = liquefaction not likely because liquefaction predicted for less than 24% of the layers analyzed.

§ See electronic supplement for detailed description of liquefaction potential analysis and tables of results.

‖ WT = water table; depth used in liquefaction potential analysis.

Table S12. Results of liquefaction potential analysis of A.D. 1200-1480 earthquake with North America plate interface northeast of Puerto Rico as source (Wei, 2022; white star on Figure 8).

Site Name	Map ID*	Distance† (km)	Results‡, § (WT@ 1 m) ‖, #	Results‡, § (WT@ 3 m) ‖
Scenario earthquake M 8.45				
Río Grande de Manatí	5	180.3	L/N	N
Río de la Plata	6	152.8	N	N
Río de la Plata	7	155.3	N	N
Río Gurabo	8	135.7	L/N	N
Río Blanco	9	128.0	L/N	L/N

* Borehole locations shown on Figure 5 and Figures S1-S5 in the Supplement.

† Distance between scenario earthquake considered and geotechnical site data used in the analysis.

‡ L = Liquefaction likely for 45% - 100% of the layers analyzed; L/N = marginal because liquefaction predicted for 24% - 44% of the layers analyzed; N = liquefaction not likely because liquefaction predicted for less than 24% of the layers analyzed.

§ See electronic supplement for detailed description of liquefaction potential analysis and tables of results.

‖ WT = water table; depth used in liquefaction potential analysis.

Table S13. Results of liquefaction potential analysis of A.D. 1304-1508 earthquake with Bowin fault zone north of Puerto Rico as source (C on Figure 8).

Site Name	Map ID*	Distance† (km)	Results‡, § (WT@ 1 m) ‖, #	Results‡, § (WT@ 3 m) ‖
Scenario earthquake M 8.0				
Río Culebrinas	1	101.7	N	N
Río Grande de Añasco	2	111.0	L	L
Río Grande de Añasco	3	112.1	L/N	N
Río Grande de Manatí	5	84.4	L	L
Río de la Plata	6	92.6	N	N
Río de la Plata	7	96.0	N	N
Río Gurabo	8	133.4	N	N
Río Blanco	9	144.3	N	N
Scenario earthquake M 8.25				
Río Culebrinas	1	101.7	L	N
Río Grande de Añasco	2	111.0	L	L
Río Grande de Añasco	3	112.1	L	L
Río Grande de Manatí	5	84.4	L	L
Río de la Plata	6	92.6	L	N
Río de la Plata	7	96.0	N	N
Río Gurabo	8	133.4	L/N	N
Río Blanco	9	144.3	N	N

* Borehole locations shown on Figure 5 and Figures S1-S5 in the Supplement.

† Distance between scenario earthquake considered and geotechnical site data used in the analysis.

‡ L = Liquefaction likely for 45% - 100% of the layers analyzed; L/N = marginal because liquefaction predicted for 24% - 44% of the layers analyzed; N = liquefaction not likely because liquefaction predicted for less than 24% of the layers analyzed.

§ See electronic supplement for detailed description of liquefaction potential analysis and tables of results.

‖ WT = water table; depth used in liquefaction potential analysis.

Table S14. Results of liquefaction potential analysis of 1201-410 B.C. earthquake with Bowin fault zone as source (C on Figure 8).

Site Name	Map ID*	Distance† (km)	Results‡, § (WT@ 1 m) ‖, #	Results‡, § (WT@ 3 m) ‖
Scenario earthquake M 7.6				
Río Culebrinas	1	101.7	N	N
Río Grande de Añasco	2	111.0	N	N
Río Grande de Añasco	3	112.1	N	N
Río Grande de Manatí	5	84.4	L	N
Río de la Plata	6	92.6	N	N
Río de la Plata	7	96.0	N	N
Río Gurabo	8	133.4	N	N
Río Blanco	9	144.3	N	N
Scenario earthquake M 7.8				
Río Culebrinas	1	101.7	N	N
Río Grande de Añasco	2	111.0	L	N
Río Grande de Añasco	3	112.1	N	N
Río Grande de Manatí	5	84.4	L	L
Río de la Plata	6	92.6	N	N
Río de la Plata	7	96.0	N	N
Río Gurabo	8	133.4	N	N
Río Blanco	9	144.3	N	N

* Borehole locations shown on Figure 5 and Figures S1-S5 in the Supplement.

† Distance between scenario earthquake considered and geotechnical site data used in the analysis.

‡ L = Liquefaction likely for 45% - 100% of the layers analyzed; L/N = marginal because liquefaction predicted for 24% - 44% of the layers analyzed; N = liquefaction not likely because liquefaction predicted for less than 24% of the layers analyzed.

§ See electronic supplement for detailed description of liquefaction potential analysis and tables of results.

‖ WT = water table; depth used in liquefaction potential analysis.

Table S15. Results of liquefaction potential analysis of 1201-410 B.C. earthquake with GNPRFZ south of Mantí as source (D on Figure 8).

Site Name	Map ID*	Distance† (km)	Results‡, § (WT@ 1 m) ‖, #	Results‡, § (WT@ 3 m) ‖
Scenario earthquake M 6.2				
Río Culebrinas	1	70.5	N	N
Río Grande de Añasco	2	64.8	N	N
Río Grande de Añasco	3	66.5	N	N
Río Grande de Manatí	5	20.0	L	L/N
Río de la Plata	6	33.4	N	N
Río de la Plata	7	30.3	N	N
Río Gurabo	8	62.8	N	N
Río Blanco	9	76.8	N	N

* Borehole locations shown on Figure 5 and Figures S1-S5 in the Supplement.

† Distance between scenario earthquake considered and geotechnical site data used in the analysis.

‡ L = Liquefaction likely for 45% - 100% of the layers analyzed; L/N = marginal because liquefaction predicted for 24% - 44% of the layers analyzed; N = liquefaction not likely because liquefaction predicted for less than 24% of the layers analyzed.

§ See electronic supplement for detailed description of liquefaction potential analysis and tables of results.

‖ WT = water table; depth used in liquefaction potential analysis.

Figures

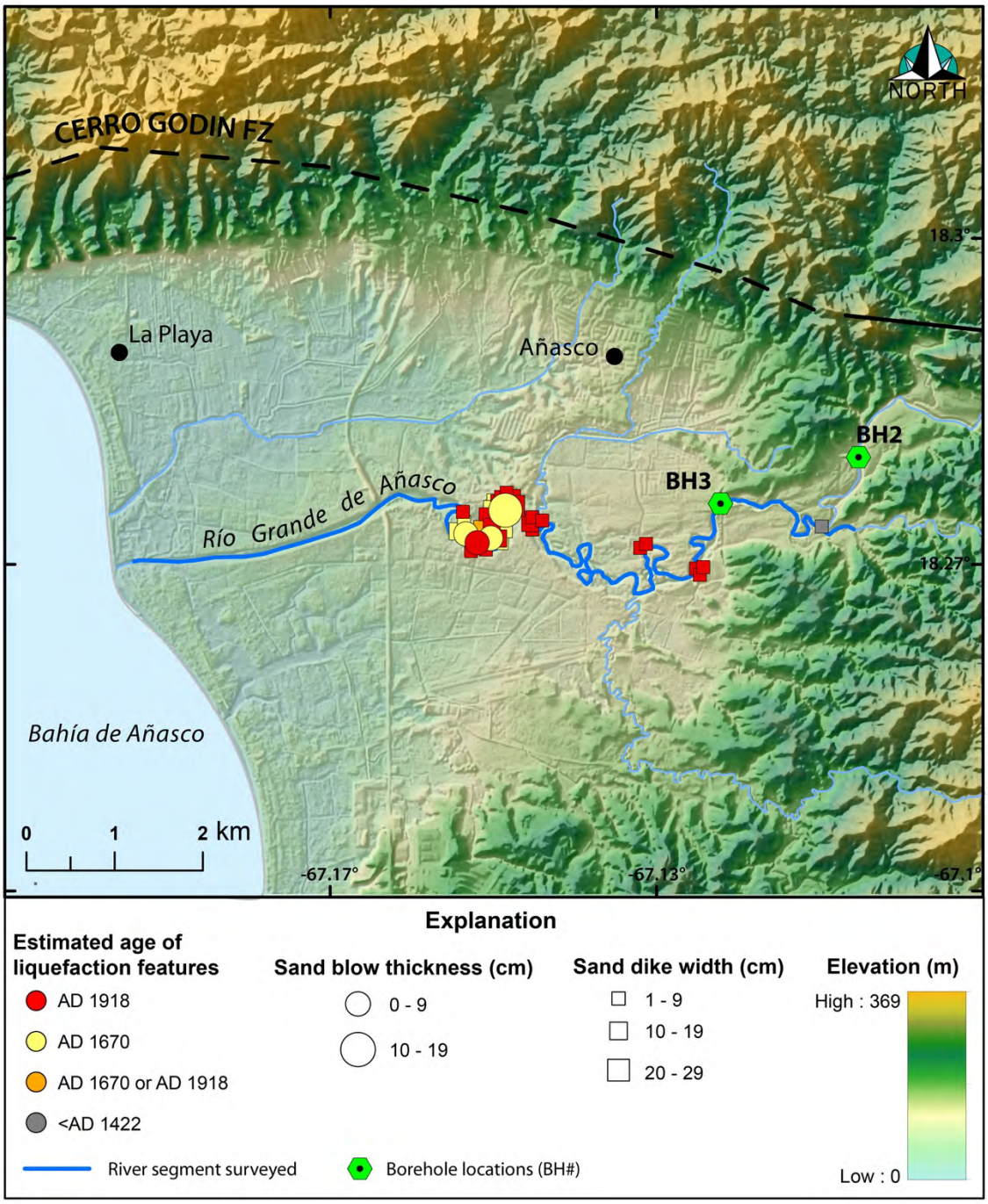

Figure S1. Map showing locations, sizes, and estimated ages liquefaction features along Río Grande Añasco.

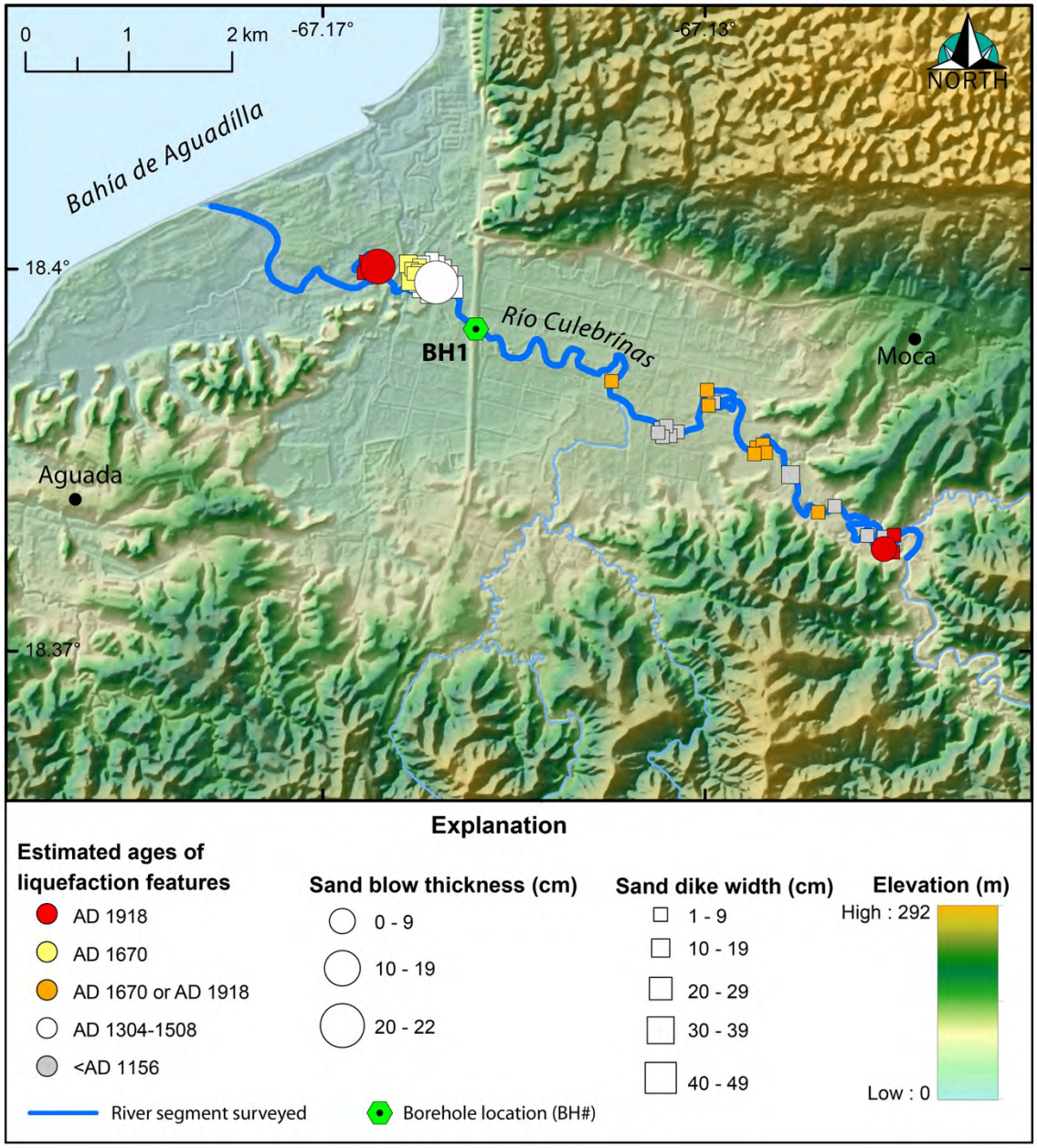

Figure S2. Map showing locations, sizes, and estimated ages liquefaction features along Río Culebrinas.

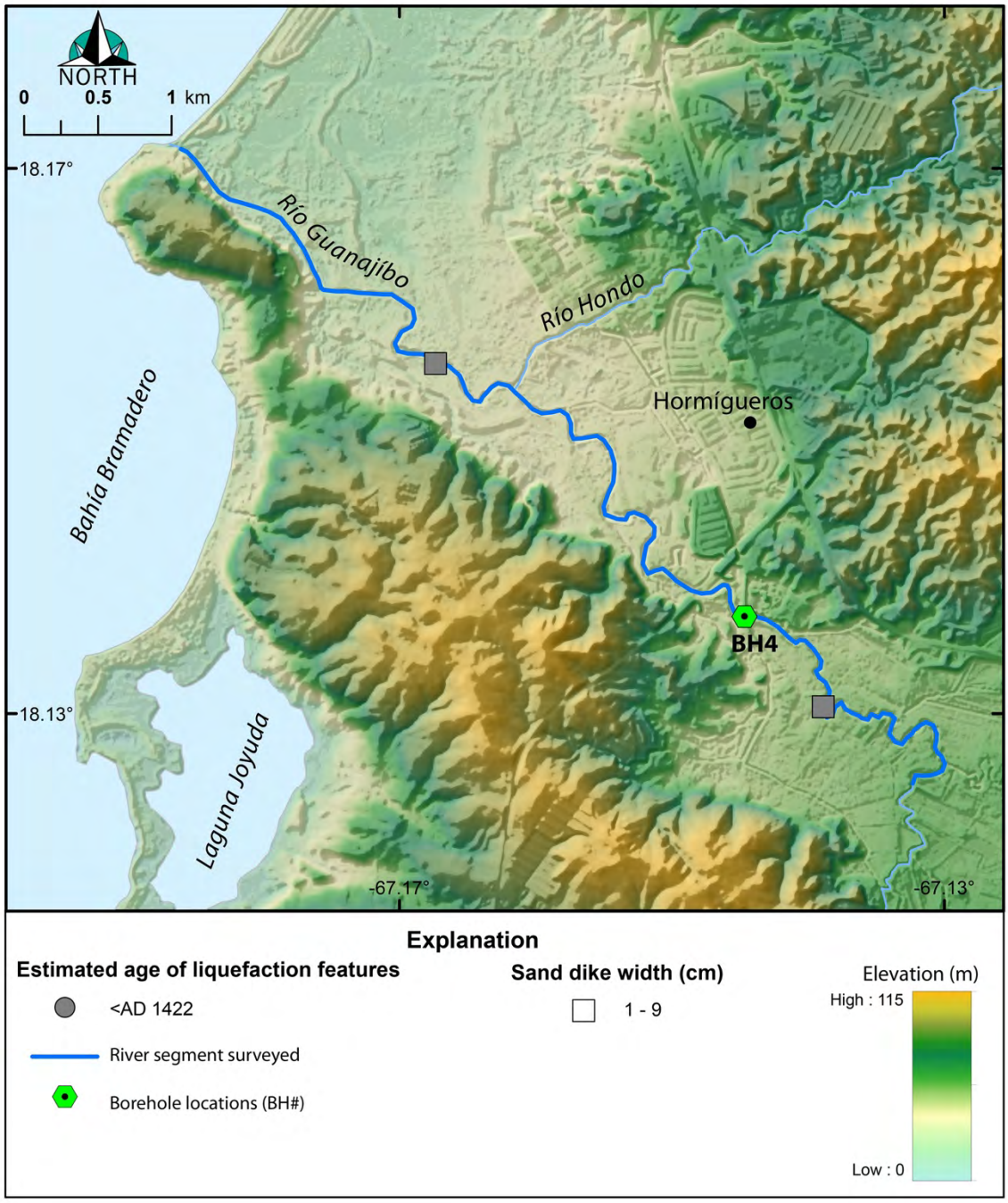

Figure S3. Map showing locations, sizes, and estimated ages liquefaction features along Río Guanajibo.

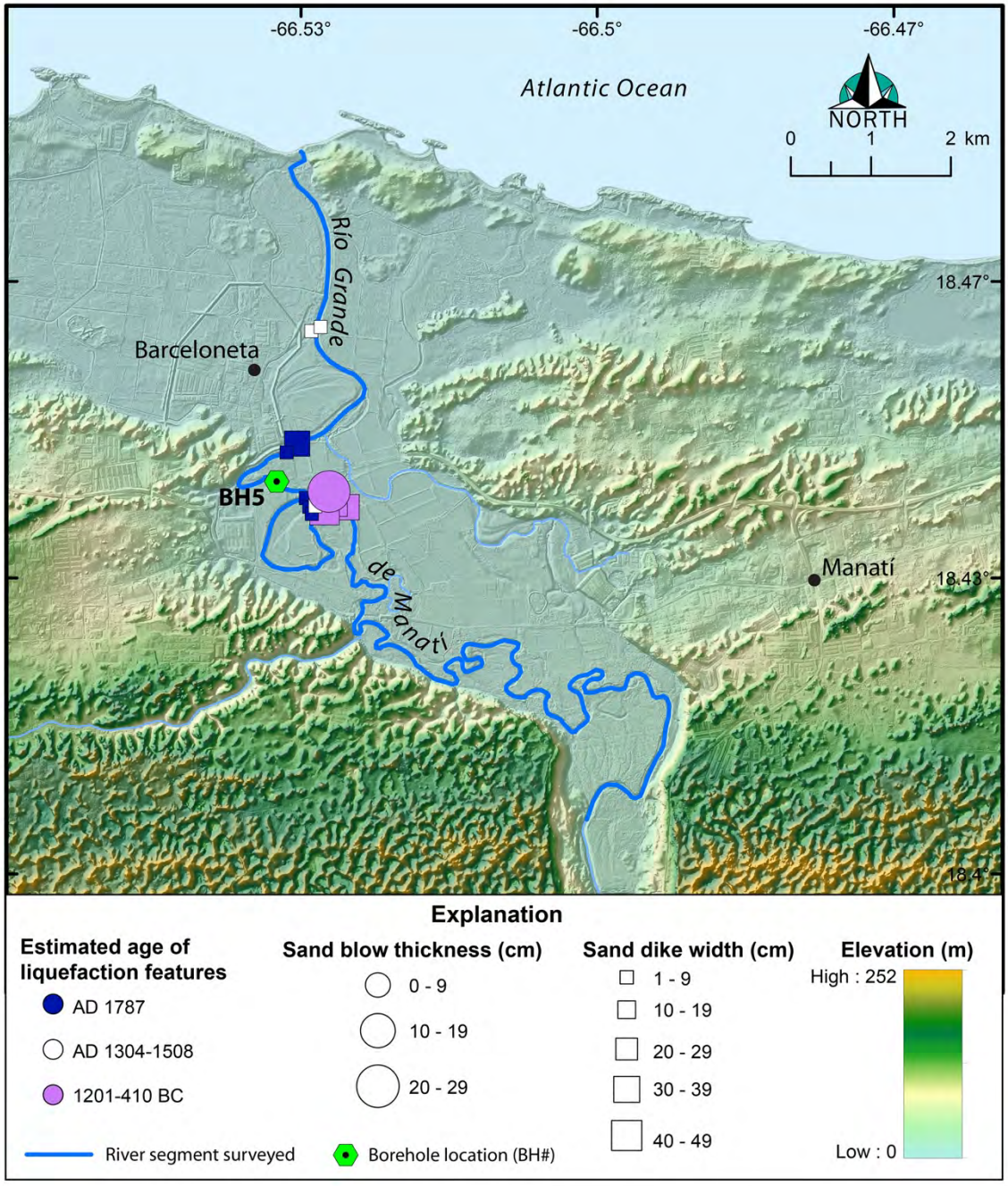

Figure S4. Map showing locations, sizes, and estimated ages liquefaction features along Río Grande de Manatí.

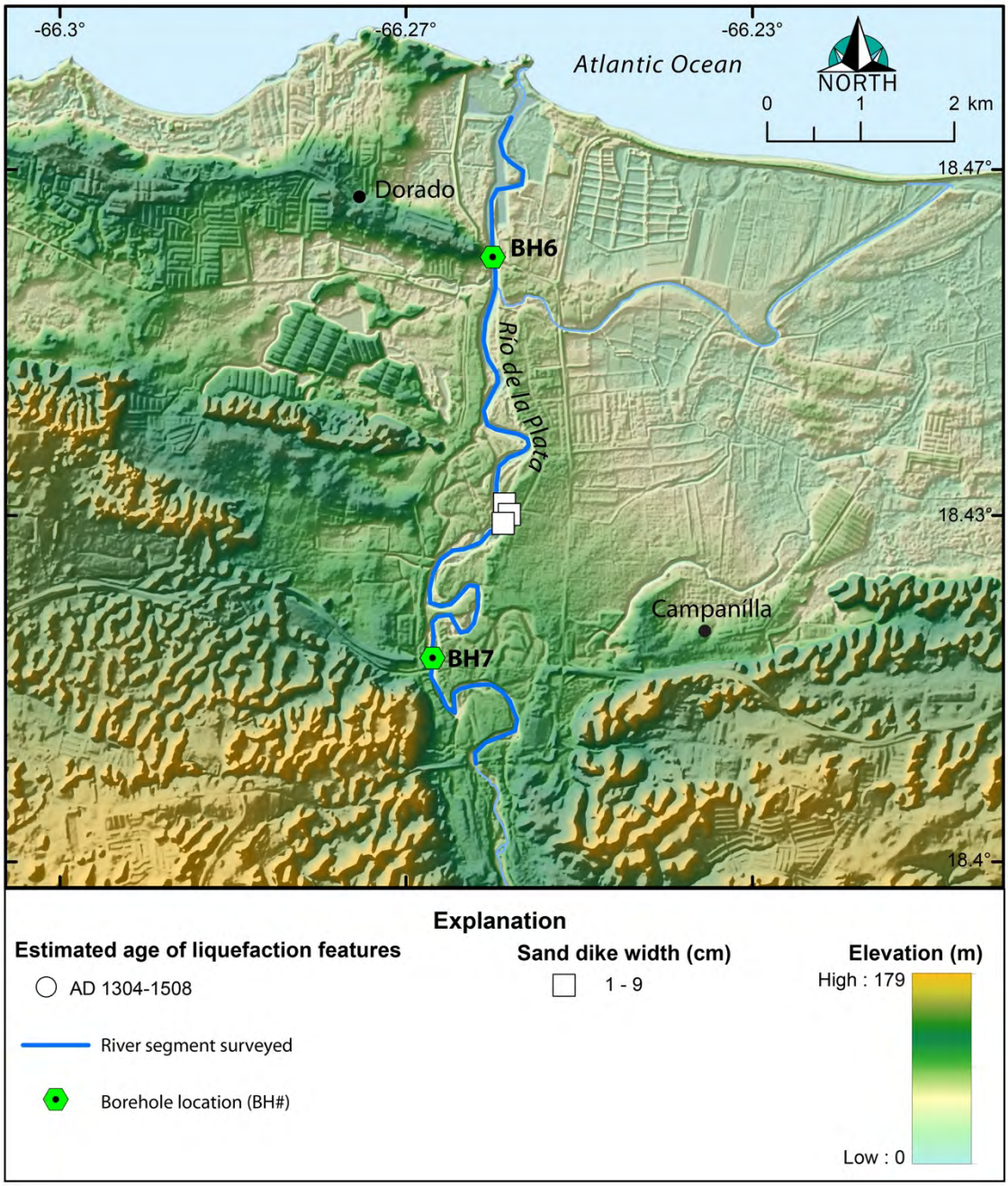

Figure S5. Map showing locations, sizes, and estimated ages liquefaction features along Río de la Plata.

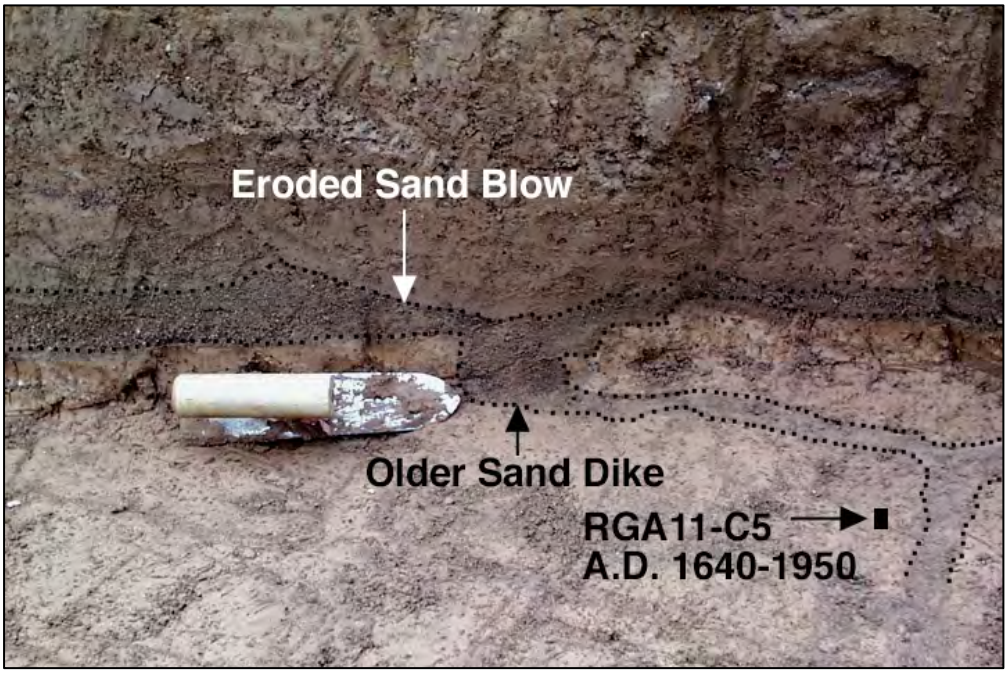

Figure S6. At site RGA11, eroded sand blow and related feeder dike. Dating of sample RGA11-C5 indicates these liquefactions and younger crosscutting dikes formed after A.D. 1640. For scale, scraper is 19 cm long.

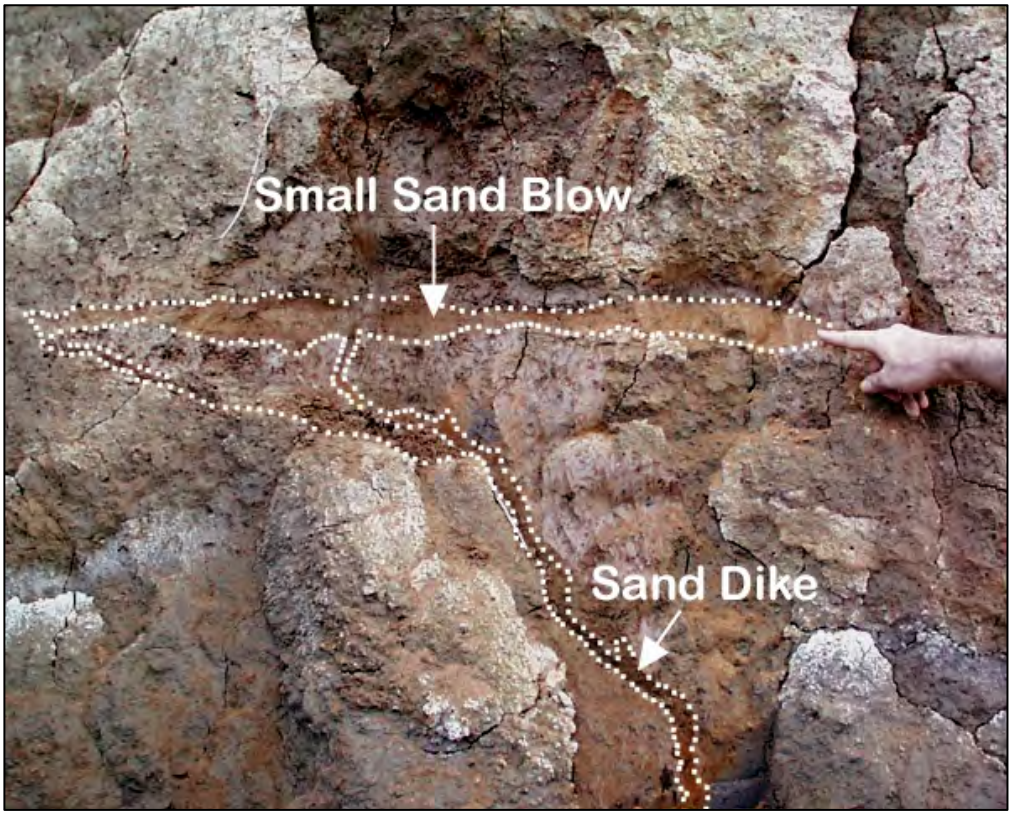

Figure S7. At site RGA16, weathered sand dike and related sand blow thought to have formed during 1670 earthquake.

Figure S8. At site RC100, sand dike pinches and terminates upsection. Upper part of dike is iron stained but loose. Age of dike is poorly constrained but formed after A.D. 1296 based on dating of sediment at nearby site RC3. For scale, shovel is 50 cm long and red and white sections represent 10 cm.

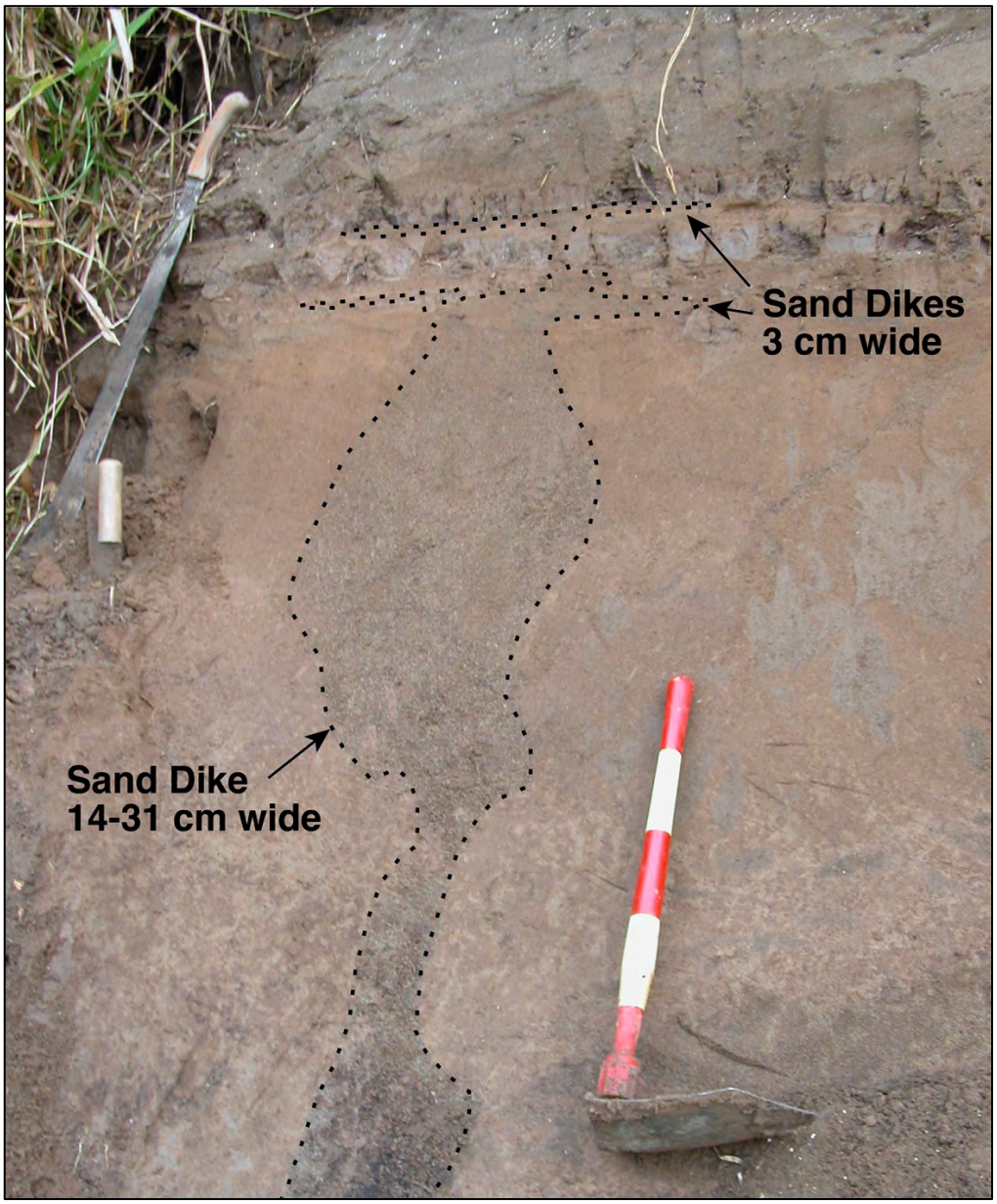

Figure S9. At site RGM5N, sand dike extends upsection where sand sills formed beneath layers of clay. Sills and upper part of dike are loose and only slightly iron stained, suggesting they are historical in age and may have formed during 1787 earthquake. Dating at nearby site RGM4N provides maximum age constraint of A.D. 1038-1216. For scale, shovel is 50 cm long and red and white sections represent 10 cm.

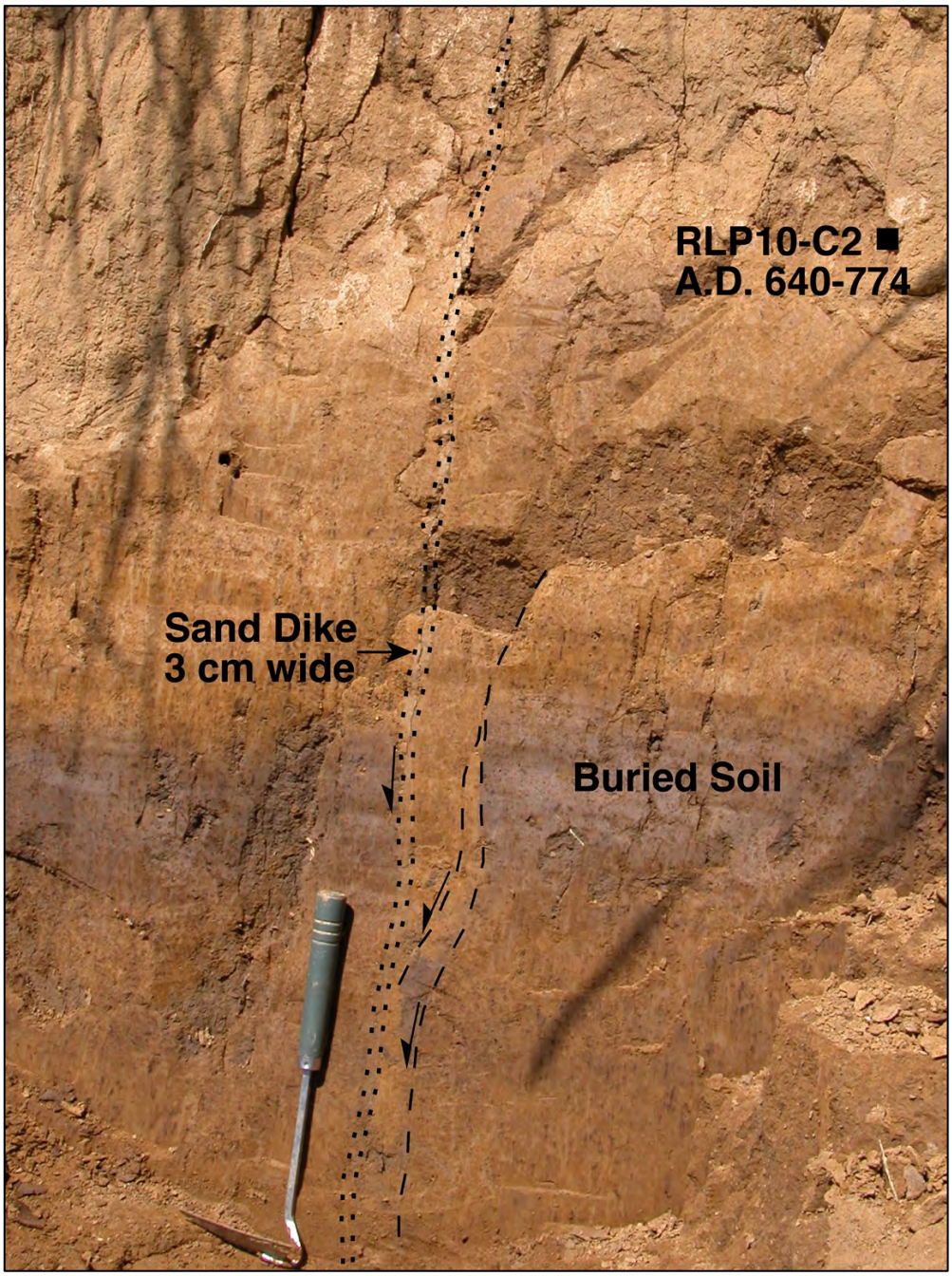

Figure S10. At site RLP10, sand dike crosscuts buried soil and extends another 60 cm in overlying silt. Graben formed in buried soil adjacent to sand dike, suggesting small amount of lateral spreading. Dike is very iron stained and mottled suggesting it is prehistorical in age. Dating of sample RLP-C2 in indicates dike formed after A.D. 640. For scale, scraper is 32 cm long.

References Cited in the Supplement

Bronk Ramsey, C., 2009, Bayesian analysis of radiocarbon dates, Radiocarbon, v. 51, n. 1, p. 337-360.

Building Seismic Safety Council, 1997, NEHRP recommended provisions for seismic regulations for new buildings and other structures, FEMA 302, Part 1 Provisions, Prepared for the Federal Emergency Management Agency, Washington, D.C.

Dobry, R., R.D. Borcherdt, C.B. Crouse, I.M. Idriss, et al., 2000, New site coefficients and site classification system used in recent building seismic code provisions, Earthquake Spectra, v. 16, p. 44-67.

Green, R. A., S. F. Obermeier, S. M. Olson, 2005, Engineering geologic and geotechnical analysis of paleoseismic shaking using liquefaction effects, Engineering Geology, v. 76, p. 263-293.

Hua, Q., M. Barbetti, and A. Z. Rakowski, 2013, Atmospheric radiocarbon for the period 1950-2010, Radiocarbon, v. 55, n. 4, p. 2059-2072. doi:10.2458/azu_js_rc.v55i2,16177

Juang, C. H., and T. Jiang, 2000, Assessing probabilistic methods for liquefaction potential evaluation, Soil Dynamics and Liquefaction 2000, GSP 107 (Proceedings GeoDenver), American Society of Civil Engineers, Reston, VA.

Mueller, C. S., A. D. Frankel, M. D. Petersen, and E. V. Leyendecker, 2003, Documentation for 2003 USGS seismic hazard maps of Puerto Rico and the U.S. Virgin Islands, USGS, Golden, Colorado, http://eqhazmaps.usgs.gov/html/prvi2003.html.

Olson, S. M., R.A.Green, and S.F. Obermeier, 2005, Revised magnitude bound relation for the Wabash Valley seismic zone of the central United States, Seismological Research Letters, v. *76*, p. 756–771. doi:10.1785/gssrl.76.6.756.

Reimer P.J., E. Bard, A. Bayliss, J.W. Beck et al., 2013, IntCal13 and MARINE13 radiocarbon age calibration curves 0-50000 years cal BP, Radiocarbon, v. 55, n. 4., p. 1869-1887. DOI: 10.2458/azu_js_rc.55.16947

Reimer P. J., W. E. N. Austin, E. Bard, A. Bayliss, et al., 2020, The IntCal20 northern hemisphere radiocarbon age calibration curve (0-55 cal kBP), Radiocarbon, v. 62, n. 4, p. 725-757. doi: 10.1017/RDC.2020.41

Seed, H. B. and I. M. Idriss, 1971, Simplified procedure for evaluating soil liquefaction potential. Journal of the Soil Mechanics & Foundations Division (ASCE), v. 97 (SM9), p. 1249-1273.

Seed, H.B., and I.M. Idriss, 1982, Ground motions and soil liquefaction during earthquakes, Earthquake Engineering Research Institute, Berkley, 134 p.

Seyhan, E., 2015, NGA-West2 GMPEs validation tool, PEER, Berkley, CA.

ten Brink, U. S., W. H. Bakun, and C. H. Flores, 2011, Historical perspective on seismic hazard to Hispaniola and the northeast Caribbean region, J. Geophys. Res., v. 116, B12318, doi:10.1029/2011JB008497.

Tuttle, M. P., Dyer-Williams, K., Schweig, E. S., Prentice, C. S., Moya, J. C., and Tucker, K. B., 2005, Liquefaction induced by historic and prehistoric earthquakes in western Puerto Rico, *in* Mann, P., ed., Active tectonics and seismic hazards of Puerto Rico, the Virgin Islands, and offshore areas: Geological Society of America Special Paper 385, p. 263-276.

Tuttle, M. P., Hartleb, R., Wolf, L., and P. W. Mayne, 2019, Paleoliquefaction studies and the evaluation of seismic hazard, Geosciences, v. 9, n. 7, 61 p, doi:10.3390/geosciences9070311.

Tuttle, M. P., Dyer-Williams, K., Carter, M. W., Forman, S. L., Tucker, K., Fuentes, Z., Velez, C., and Bauer, L. M., 2021, The liquefaction record of past earthquakes in the Central Virginia seismic zone, Eastern United States, Seismological Research Letters, v. 92, p. 3126-3144, plus electronic supplement, doi: https://doi.org/10.1785/0220200456.

U.S. Geological Survey, Earthquake Hazards Program, 2017, Advanced National Seismic System (ANSS) comprehensive catalog of earthquake events and products: various, https://doi.org/10.5066/F7MS3QZH.

Wei, Y., 2022, Evaluating outer-rise earthquake hazards from the Puerto Rico Trench by calibrating inundation models with geologic evidence, Final Technical Report, Earthquake Hazard Reduction Program Award No. G20AP00049, p. 53, plus supplement.

Youd, T.L., et al., 2001, Liquefaction resistence of soils: Summary report from the 1996 NCEER and 1998 NCEER/NSF workshops on evaluation of liquefaction resistence of soils, Journal of Geotechnical and Geoenvironmental Engineering, v. 127, n. 10, p. 817-833.

Youd, T. L., and I. M. Idriss, 2003, Liquefaction resistance of soils: Summary report from the 1996 NCEER and 1998 NCEER/NSF workshops on evaluation of liquefaction resistance of soils: Closure and Errata, Journal of Geotechnical and Geoenvironmental Engineering, v. 129, n. 3, 285 p.